2009

Clamping of Intracellular pH in Neurons from Neonatal Rat Brainstem during Hypercapnia

Vivian C. Nanagas
Wright State University

CLAMPING OF INTRACELLULAR pH IN NEURONS FROM NEONATAL RAT BRAINSTEM DURING HYPERCAPNIA

A thesis submitted in partial fulfillment
of the requirements for the degree of
Master of Science

By

VIVIAN CRUZ NANAGAS
B.A., University of Notre Dame, 2007

2009
Wright State University

WRIGHT STATE UNIVERSITY

SCHOOL OF GRADUATE STUDIES

June 29, 2009

I HEREBY RECOMMEND THAT THE THESIS PREPARED UNDER MY SUPERVISION BY Vivian Cruz Nanagas ENTITLED Clamping of Intracellular pH in Neurons from Neonatal Rat Brainstem during Hypercapnia BE ACCEPTED IN PARTIAL FULFILLMENT OF THE REQUIREMENTS FOR THE DEGREE OF Master of Science.

_____

Robert W. Putnam, Ph.D.
Thesis Director

_____

Timothy C. Cope, Ph.D.
Department Chair

Signatures of Committee
on Final Examination

_____

Robert W. Putnam, Ph.D.

_____

Christopher N. Wyatt, Ph.D.

_____

Lynn K. Hartzler, Ph.D.

_____

Joseph F. Thomas, Jr., Ph.D.
Dean, School of Graduate Studies

ABSTRACT

Nanagas, Vivian Cruz. M.S., Department of Neuroscience, Cell Biology and Physiology, Wright State University, 2009. Clamping of Intracellular pH in Neurons from Neonatal Rat Brainstem during Hypercapnia.

In this work, I have made attempts to clamp intracellular pH in the presence of hypercapnic acidosis (HA) in neurons from the locus coeruleus (LC) and nucleus of the solitary tract (NTS) in neonatal rat (ages P3 to P17) brainstem slices. Two approaches were used to minimize hypercapnia-induced ΔpH_i: 1) an increase in intracellular buffering power with a high HEPES concentration using whole cell patching techniques in individual neurons, and 2) a weak acid diffusion technique that relies on an efflux of weak acid to counterbalance HA influx thereby clamping pH_i in multiple neurons at once. pH_i was measured using two pH-sensitive fluorescent dyes: membrane impermeable pyranine for the former approach, and the acetoxymethyl ester form of membrane permeable 2',7'-bis-(2-carboxyethyl)-5-(and-6)-carboxyfluorescein (BCECF) for the latter. Blunting with HEPES buffer was performed in the NTS only, with a calculated average percent blunting of hypercapnia-induced acidification of 73.4%. Experiments blunting via weak acid diffusion utilized an inverted microscope and two weak acids: acetic acid and caproic (hexanoic) acid. In NTS neurons (n=56), acetic acid blunted acidification by only 33.1% and in LC neurons by only 19.6% (n=52). Caproic acid blunted hypercapnia-induced acidification by 50.7% (n=58) and 45.8% (n=47) in NTS and LC neurons, respectively. Experiments were also repeated using an upright microscope. In these experiments, acidification was blunted by 45.8% (n=56) and 52.6%

(n=52) in NTS and LC neurons, respectively. Concurrent influx of weak base, trimethyl amine, with HA was also used to blunt ΔpH_i, but the results showed no blunting and, in fact, a greater acidification in response to HA: -18.1% in the NTS (n=40) and -27.8% in the LC (n=28). These techniques are clearly insufficient to accomplish a complete clamping of hypercapnia-induced changes in pH_i. However, we have determined that the ability to clamp pH_i is highly affected by diffusion of the weak acid both up to and into the cell. Blunting could be improved with better superfusion of slices and the use of more permeable weak acids. Overall, the ability to blunt ΔpH_i, especially in numerous cells simultaneously, would be valuable in studying systems where pH_i may play a role in cellular function, such as the involvement of pH_i in chemosensitive signaling, bicarbonate reabsorption in the proximal tubule, free fatty acid diffusion in adipocytes, and acid-sensing taste receptors.

TABLE OF CONTENTS

TABLE OF CONTENTS (CONT'D.)

LIST OF FIGURES

Page

LIST OF FIGURES (CONT'D)

LIST OF FIGURES (CONT'D)

ACKNOWLEDGEMENTS

I would like to thank first and foremost Dr. Robert W. Putnam for being my advisor, mentor, teacher, and friend who has been one of the most inspirational figures in my life. Next, I would like to thank my committee members Drs. Chris Wyatt and Lynn Hartzler for their support, encouragement, insight, and guidance. I wish to thank Dr. Hartzler especially for being with me from the very beginning, even before my thesis project, for her patience, time, knowledge, and personal attention. I would also like to thank all the Putnam lab members past and present for making work fun and for all their real-time support! Last but not least, thanks go to my family, friends, and Jeremy for always thinking the best of me.

CHAPTER I

INTRODUCTION

Intracellular pH (pH_i) is an important attribute of all living cells and a fundamental component of their physiological environment. Cells depend on and function within a fairly narrow pH range and even relatively small pH variations could significantly alter normal cell functioning. Thus, it is not surprising that nearly all cells possess mechanisms, from intracellular buffering to pH-regulating membrane transporters, that allow them to minimize and recover from acid/base insults.

There are a number of cells, however, for which a change of pH_i is not a pathological disruption of cell function but an intracellular signal and part of the normal response of the cell to some appropriate stimulus. An example of such pH-sensing cells are the central and peripheral chemoreceptors that sense fluctuating levels of CO_2/H^+ and contribute to the regulation of ventilation. For example, in central chemosensitive neurons, CO_2/H^+-induced changes in firing rate have been postulated to be mediated by changes in pH_i (Lassen, 1990; Putnam et al., 2004), although an alternative model has been proposed in which changes of pH_i are just one of many possible chemosensitive signals, no one of which is necessary for the chemosensitive response (Putnam et al., 2004). Further, central chemosensitive neurons are believed to reside in several brainstem regions, including the medullary nucleus tractus solitarius (NTS) and the pontine locus coeruleus (LC). It is highly likely that chemosensitive signaling differs in neurons from these different regions (Martino and Putnam, 2007). In order to study the involvement of changes of intracellular pH_i in chemosensitive signaling in these neurons, it would be of use to have a technique to clamp pH_i in the face of acid challenges.

We have had some initial success with pH_i clamping in LC neurons (Hartzler et al., 2008) but in this thesis I want to extend these studies to develop the ability to clamp

or blunt pH_i changes in NTS neurons in response to acid loads and to develop the ability to clamp/blunt pH_i changes in numerous cells within a brainstem slice, not just a single patch-clamped neuron. We anticipate that such techniques will not only be useful to the study of chemosensitive neurons but also in other cell models where changes of pH_i are likely to play a signaling role, such as acid-sensing taste receptors that give rise to sour taste, nociceptive cells, and renal proximal tubule cells that regulate the compensatory renal response to blood acid-base disturbances.

CHAPTER II

LITERATURE REVIEW

Intracellular pH in Cells

Most cells maintain an intracellular pH (pH_i) that is alkaline relative to H^+ equilibrium. This value of pH_i can be important for nearly all cellular processes since changes of pH can alter the structure of proteins and lipids and thus affect the function of these compounds (for review see Putnam and Roos, 1997). A cell can respond to pH challenges in two main ways: either with internal buffering power or through a variety of membrane transporters. Buffering power can minimize the effects of an acid/base disturbance but cannot lead to recovery from that disturbance. In other words, the effect of an acid challenge on pH_i can be reduced by a high intracellular buffering power but the cell will still acidify to some degree. On the other hand, true pH_i regulation in the face of acid/base challenges can only be achieved through the mediation of various membrane transporters. Most of these transporters can be divided into one of two types. The first are Na^+/H^+ exchangers that use the Na^+ gradient to extrude internal H^+, thus mediating alkalinizing recovery from an acid load (for review see Orlowski and Grinstein, 2004). The other main group of transporters comprises a variety of HCO_3-dependent transporters which can transport the base HCO_3 either into (alkalinizing) or out of (acidifying) the cell, contributing to the regulation of pH_i from either an acid or an alkaline challenge (for review see Romero et al., 2004).

Although most cells want to maintain a constant pH_i to maintain proper cell function, there are a number of cells for which a change of pH_i is an intracellular signal and part of the normal response of the cell to external stimuli. Examples of such cells include taste bud receptors that give rise to sour taste (Stewart et al., 1999; DeSimone et al., 2001), pain-sensing nociceptors (Wegner et al., 1996), and renal proximal tubule cells

that contribute to renal compensation of blood acid/base disturbances (Zhao et al., 2003). However, some of the best examples of putative pH sensing cells are the central and peripheral chemoreceptors that sense altered levels of CO_2/H^+ and modulate ventilation to lead to respiratory compensation for blood acid/base disorders (Putnam et al., 2004). In all of these cells, in order to study the involvement of changes of intracellular pH in the signaling mechanism, it would be of use to have a technique to clamp pH_i in the face of an acid challenge. In this thesis, I have focused on developing such techniques for neurons believed to be involved in central respiratory control.

Central Respiratory Control

Breathing originates from cellular mechanisms in the brainstem, a process involving the integration of neural signals and resulting in a basic rhythm of inspiration and expiration. Although its precise molecular workings are still far from known, respiration is largely thought to be controlled by several anatomical regions including the pontine respiratory group, the pre-Bötzinger complex, the Bötzinger complex (BötC), and the dorsal and ventral respiratory groups of the medulla (Figure 1), where focal acidification, inhibition, and lesions of these areas alter ventilatory components such as tidal volume, frequency, and the generation of a respiratory rhythm (Fung and St. John, 1994; Mizusawa et al., 1995; Nattie, 1999; Alheid et al., 2004; Krause et al., 2009; Song and Poon, 2009). Within this brainstem respiratory network, two specific areas were used for the work in this thesis, having been well identified as participants in the respiratory process: the locus coeruleus (LC) (Li et al., 1992; Oyamada et al., 1998; Ritucci et al., 1998; Filosa et al., 2002; Ballantyne et al., 2004; Biancardi et al., 2008; Hartzler et al., 2008; Nichols et al., 2008) and the nucleus of the solitary tract (NTS) (Dean et al., 1989;

FIGURE 1: Dorsal view showing neuroanatomy of the brainstem respiratory network with cerebellum removed. Abbreviations: BC: Bötzinger complex; cVRG: caudal ventral respiratory group; K-F: Kölliker-Fuse nuclerus; LC: locus coeruleus; NTS: nucleus tractus solitarii/nucleus of the solitary tract; PB: parabrachial nucleus; PBC: pre-Bötzinger complex; RTN/pFRG: retrotrapezoid nucleus and parafacial respiratory group; and rVRG: rostral ventral respiratory group. From Spyer MK., *Exp Physiol*. 94:1-10, 2009.

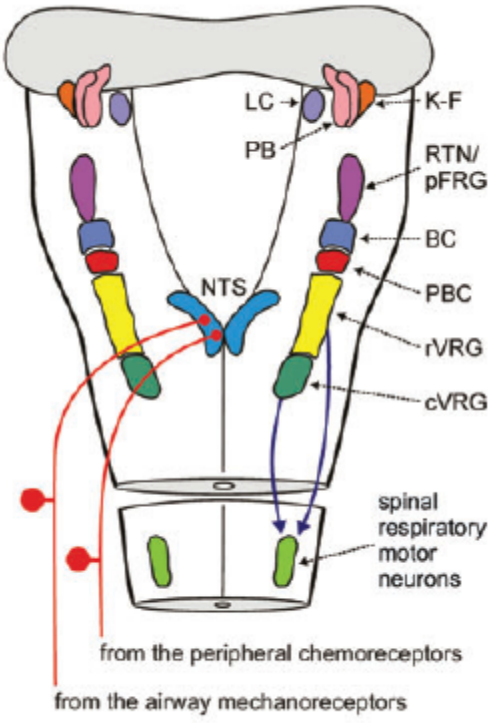
LC
K-F
PB
RTN/
pFRG
BC
NTS
PBC
rVRG
cVRG
spinal
respiratory
motor
neurons
from the peripheral chemoreceptors
from the airway mechanoreceptors

Dean et al., 1990; Coates et al., 1993; Dean et al., 1997; Ritucci et al., 1998; Mulkey et al., 2003; Conrad et al., 2009; Nichols et al., 2009) (Figure 2). LC and NTS neurons are believed to play a role as central chemoreceptors, sensing fluctuating levels of CO_2 in the body that are, in part, responsible for the chemical feedback regulating ventilatory control. This capacity to respond to elevated levels of CO_2/H^+ is a property known as chemosensitivity, mediating a complex signaling mechanism that, despite considerable research, is also not yet fully characterized but described in part below.

Central Chemosensitivity and pH

Central chemoreceptors detect changes in increased CO_2 and/or decreases in pH. Although there are many CO_2/H^+-sensitive cells within the body, areas of central chemosensitivity are specifically defined, amongst other criteria, by eliciting an increased ventilatory response when those regions are focally acidified, or by eliciting a decreased ventilatory response to inspired hypercapnia when those regions are ablated (Nattie 2000). A central chemosensitive neuron, consequently, we define as one that exists within a chemosensitive region, significantly increases or decreases its firing rate upon hypercapnic exposure, and is intrinsically responsive to CO_2 changes (Ritucci et al., 1997; Putnam et al., 2004). To be intrinsically chemosensitive, excitability is demonstrated in the absence of all synaptic input from other chemosensitive neurons, both chemically by way of neurotransmitter release and electrically by way of existing gap junctions (Conrad et al, 2009; Leiter, 2009; Nichols et al., 2009).

The signaling mechanism by which these neurons respond to hypercapnia has been a major focus of research. The classic model describes this process as the decrease

FIGURE 2. Sagittal view of the brainstem showing multiple ventilatory control regions, cranial end facing left. Regions suggested to be involved in central chemoreception are shaded. Shown again are the locations of the locus coeruleus (LC) and nucleus of the solitary tract (NTS) employed for pH_i clamping. The caudal portion of the NTS is the area containing the respiratory neurons used in this work, circled in red. The dotted line indicates transverse slicing (see Materials and Methods). Adapted from Nattie E., *Resp. Physiol.* 122:223-235, 2000.

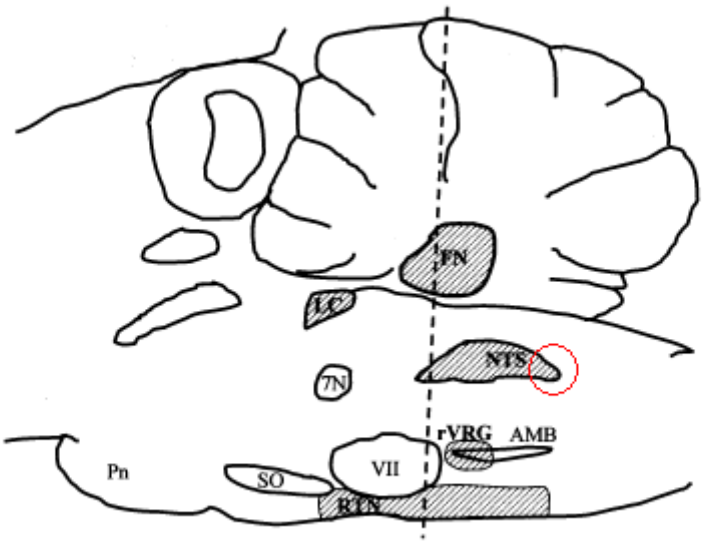
FN
LC
NTS
7N
rVRG
AMB
Pn
SO
VII
RTN

in intracellular pH due to the hydration and subsequent dissociation of diffused CO_2 into bicarbonate and free H^+. This acidification in turn could inhibit a potassium channel, which would thus increase the firing rate of the cell due to the consequent depolarization of the membrane (Figure 3) (Lassen, 1990, Putnam et al., 2004). An alternative model for central chemosensitive signaling is the recently proposed multiple factors model (Putnam et al., 2004). In this model, multiple signals, including decreased pH_i, decreased extracellular pH (pH_o), and increased intracellular calcium lead to changes of multiple ion channels, and the resultant change in firing rate in response to hypercapnia is due to the combination of all of these effects (Figure 4). The ability to clamp pH_i would be critical to differentiating these models in neurons from various chemosensitive regions (e.g. Hartzler et al., 2008).

The nature of the cellular signals in chemosensitive neurons in response to hypercapnia have been investigated, and three major signals have been presented as possibilities: increased molecular CO_2 itself, decreased intracellular pH (pH_i), and/or decreased extracellular pH (pH_o). Carbon dioxide has been shown to be sensed directly by a CO_2 receptor in renal proximal tubule cells (Zhao et al., 2003) but no such receptor has been reported for chemosensitive neurons. H^+ ions have been suggested as the chief signal for chemosensitive cells, with considerations for pH_i as the primary one (Lassen, 1990; Wiemann et al., 1998; Nattie, 1999). Of what is known currently, however, an imperfect relationship exists between changes of pH_i and firing rate in LC and RTN neurons. Upon exposure to HA, the correlation of hypercapnia-induced acidification with increased firing is poor in the RTN, and upon removal of HA, the correlation of pH_i

FIGURE 3. Diagram of the classic model of the chemosensitive response. A stimulus such as CO_2(g) diffuses across the neuron membrane. Increased levels of CO_2 drive the reaction catalyzed by carbonic anhydrase forward to form bicarbonate and H^+, decreasing intracellular pH (pH_i). This drop in pH_i alters the conformation of a K^+ channel and depolarizes the cell membrane, which leads to an increased firing rate. pH levels are also decreased outside the cell (pH_o) which affect the behavior of other transport proteins.

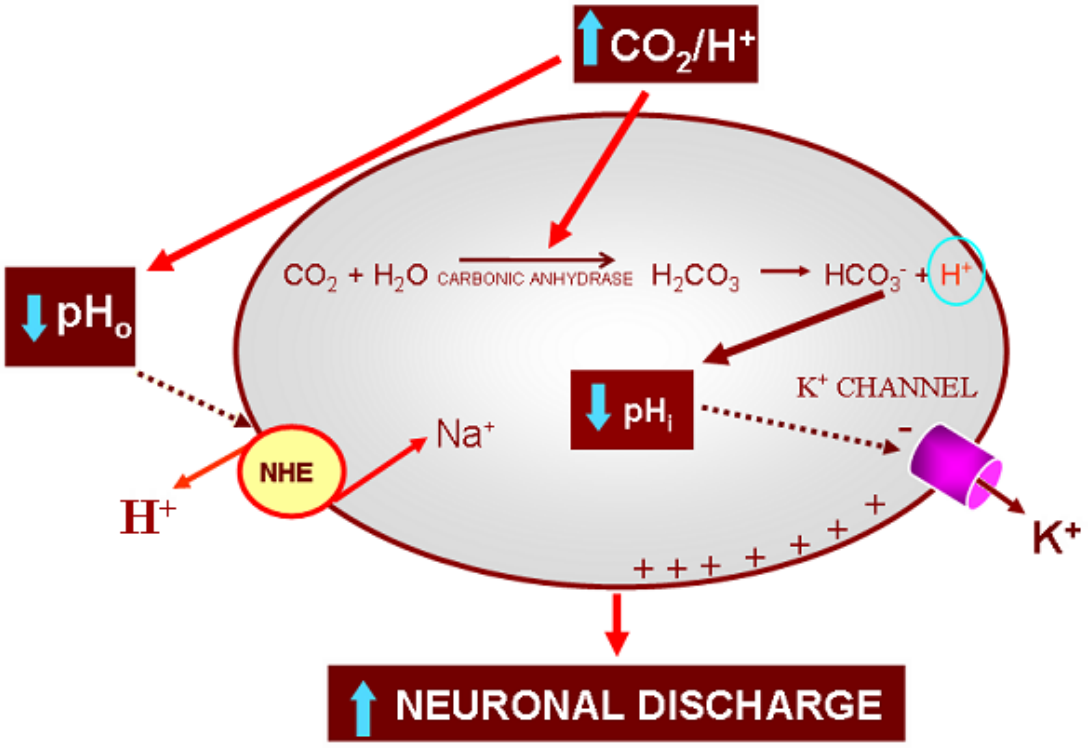
CO2/H+
pHo
CO2 + H2O
CARBONIC ANHYDRASE
H2CO3
HCO3- + H+
pHi
K+ CHANNEL
NHE
Na+
H+
K+
NEURONAL DISCHARGE

FIGURE 4: Chart of the multiple factors model. In this model, an acid stimulus (HA) manifests as several signals such as increased CO_2 and decreased pH inside and outside the cell. These signals in turn affect multiple channel targets such as L-type Ca^{2+} channels and TEA-sensitive K^+ channels. It is the sum of effects resulting from these multiple signals and multiple channels that produce the final firing rate response. Adapted from Putnam et al., *Am J. Physiol*. 287:C1493-C1526, 2004.

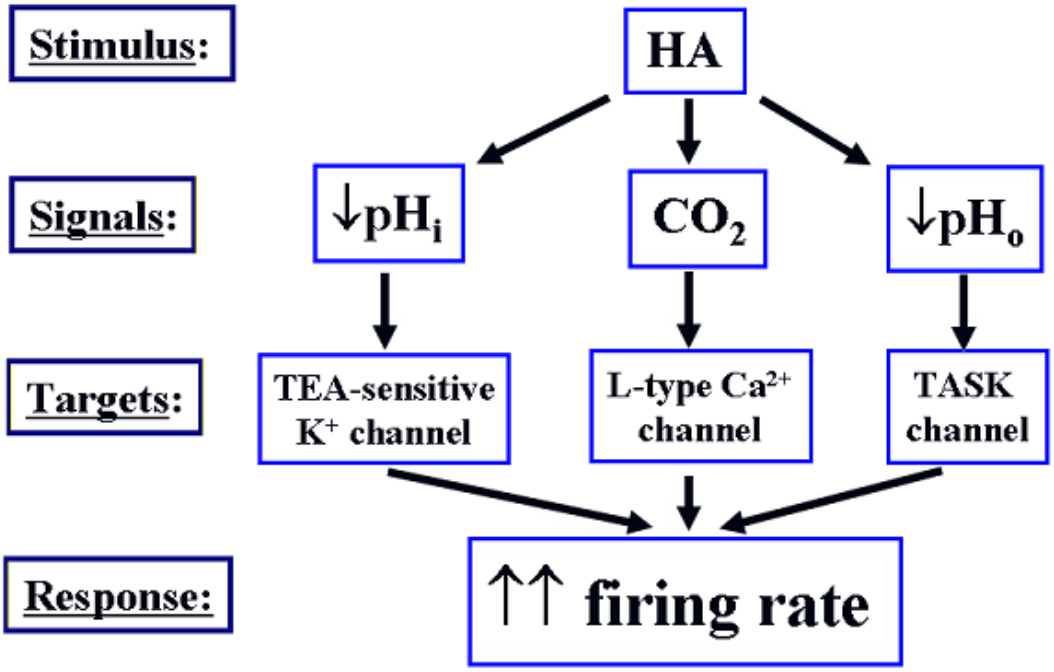
Stimulus:
HA
Signals:
↓pH$_i$
CO$_2$
↓pH$_o$
Targets:
TEA-sensitive K$^+$ channel
L-type Ca^{2+} channel
TASK channel
Response:
↑↑ firing rate

recovery with firing rate is poor in the LC (Filosa et al., 2002; Ritucci et al., 2005). Also, in the LC, it has been shown that a drop in pH_i is not required for the chemosensitive response (Hartzler et al., 2008). It would be advantageous, therefore, to have a technique for pH_i clamping that can be used in all chemosensitive neurons.

Just as many chemosensitive signals have been proposed, many ion channel targets of these signals have also been suggested to be involved in the response of chemosensitive neurons. These channels include pH-sensitive inwardly rectifying K^+ channels (Doi et al., 1996; Yang and Jiang, 1999), voltage sensitive K^+ channels (Berger et al., 1998), TWIK-related K^+ channels (Bayliss et al., 2001; Miller et al, 2004), and calcium-activated K^+ channels (Wellner-Kienitz et al, 1998), all of which demonstrate a pH-induced response which could potentially alter the firing rate. Specifically, two K-channel inhibitors, tetraethyl ammonium (TEA) and 4-aminopyridine (4AP), have been found to partially inhibit or reduce hypercapnia-induced firing rate in LC neurons (Filosa and Putnam, 2003; Martino and Putnam, 2007), while 4AP completely blocks the activated chemosensitive response in NTS neurons (Martino and Putnam, 2007). These findings suggest that different ion channels may be involved in the response of neurons from different chemosensitive regions. While the classic model mentions a potassium channel, K^+ channels may not be the only targets involved in chemosensitive signaling. Inhibition of L-type Ca^{2+} channels has been shown to reduce or even eliminate the hypercapnia-induced firing response of LC neurons (Filosa and Putnam, 2003). Calcium channels are generally inhibited by acidification in non-chemosensitive cells (Klöckner and Isenberg, 1994; Takahashi and Copenhagen, 1996; Tombaugh 1998), but have been shown to be activated by hypercapnia in LC neurons (Filosa and Putnam, 2003) and

carotid body cells (Summers et al., 2002). A technique for clamping pH_i would be most helpful for studying the basis for the inhibition or activation of various ion channels during hypercapnic acidosis.

It is easily hypothesized, therefore, that different signals or a different combination of the mentioned signals may operate depending on the regional location of the chemosensitive neuron being studied. The same is true for both the type and number of target channels involved. Whichever the case, these data have led to the proposed multiple factors model (Filosa and Putnam, 2003; Putnam et al., 2004) whereby no single stimulus and/or target is necessary for chemosensitive signaling. In this model, as mentioned previously, an acidic stimulus such as hypercapnia results in multiple signals, each acting on multiple targets, of which the overall additive effect results in an increased firing rate of the chemosensitive neuron (Figure 4).

Intracellular pH Regulation in Chemosensitive Cells

Most cells see changes in pH as a threat to cellular homeostasis and regular activity. On the other hand, we have discussed chemosensitive cells as a type of specialized cell that uses changes in the acidic environment as a signal for their major function. It is likely that these cells still, under some circumstances, need to maintain pH_i for cellular homeostasis. It has been shown that, in response to hypercapnic acidosis, neurons from chemosensitive regions do not exhibit pH_i recovery while neurons from non-chemosensitive regions do (Ritucci et al., 1997; Figure 5). This difference was shown to be due to altered sensitivity to inhibition of pH-regulating transporters by decreased pH_o, with a greater external acidification needed to prevent pH_i recovery from

FIGURE 5: Response of intracellular pH to hypercapnic acidosis in the neurons of two chemosensitive (CS) and two non-chemosensitive (non-CS) regions. A: Neuron from the inferior olive (IO). B: Neuron from the hypoglossal (Hyp) C: Neuron from nucleus tractus solitarii (NTS). D: Neuron from the ventrolateral medulla (VLM). Each neuron was exposed to bouts of normal saline buffer equilibrated first with 5% CO_2, then 10% CO_2 (i.e. hypercapnic acidosis,) then back to 5% CO_2 again. Recovery of pH_i is seen in neurons during HA from the non-CS areas (IO and Hyp), but not seen in neurons from CS areas (NTS and VLM). From Ritucci et al., *Am J Physiol.* 273:R433-41, 1997.

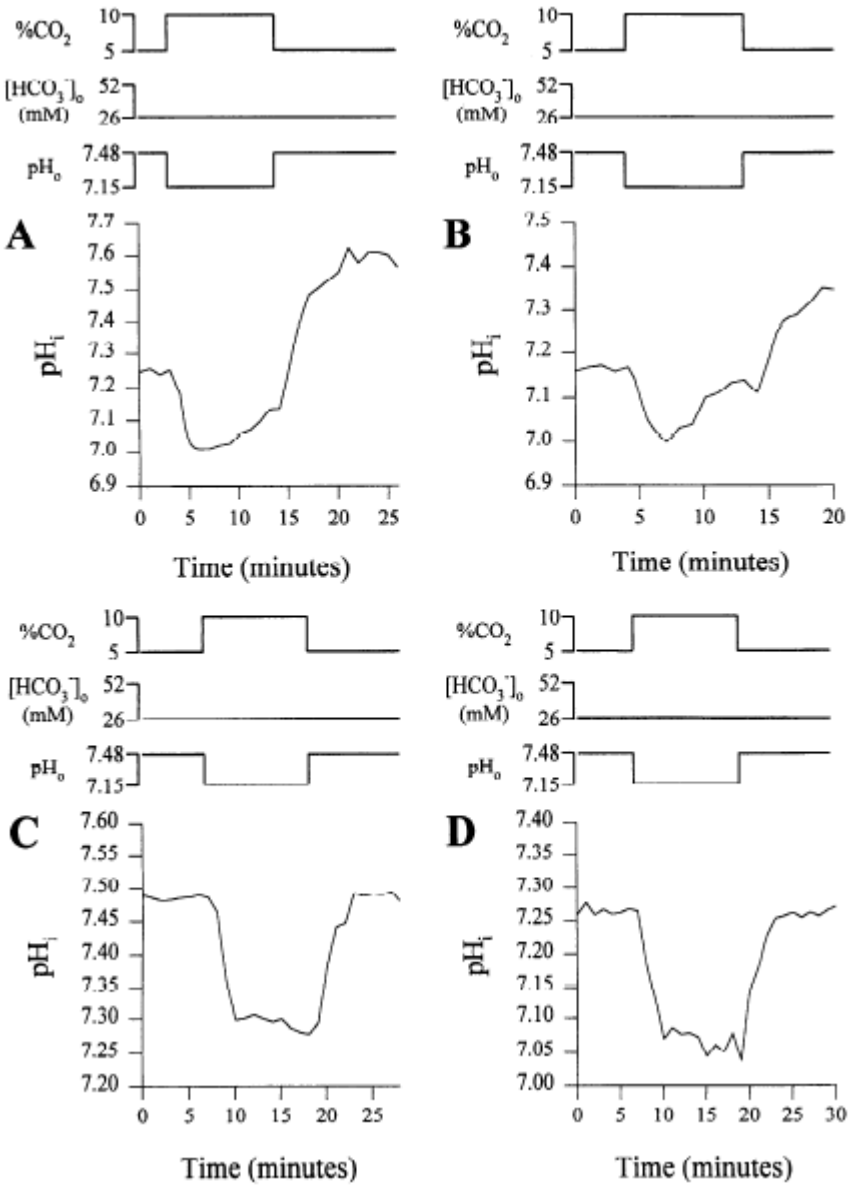
%CO2
10
5
[HCO3-]o (mM)
52
26
pHo
7.48
7.15
A
pHi
7.7
7.6
7.5
7.4
7.3
7.2
7.1
7.0
6.9
0 5 10 15 20 25
Time (minutes)
%CO2
10
5
[HCO3-]o (mM)
52
26
pHo
7.48
7.15
B
pHi
7.5
7.4
7.3
7.2
7.1
7.0
6.9
0 5 10 15 20
Time (minutes)
%CO2
10
5
[HCO3-]o (mM)
52
26
pHo
7.48
7.15
C
pHi
7.60
7.55
7.50
7.45
7.40
7.35
7.30
7.25
7.20
0 5 10 15 20 25
Time (minutes)
%CO2
10
5
[HCO3-]o (mM)
52
26
pHo
7.48
7.15
D
pHi
7.40
7.35
7.30
7.25
7.20
7.15
7.10
7.05
7.00
0 5 10 15 20 25 30
Time (minutes)

acidosis in non-chemosensitive vs. chemosensitive neurons (Ritucci et al., 1998). Nevertheless, in the absence of a decrease in external pH (e.g. with isohydric hypercapnia, made by increasing CO_2 and HCO_3 in the solution to maintain pH_o constant), all neurons display a recovery from acidification (Ritucci et al., 1998; Putnam, 2001). Thus, chemosensitive neurons do contain pH-regulating transporters, but they appear to be inhibited during hypercapnic acidosis.

The presence of pH-regulating transporters has been demonstrated in the neurons of several chemosensitive areas such as the ventrolateral medulla and NTS (Ritucci et al., 1997; Wiemann et al., 1998; Wiemann and Bingmann 2001), the RTN (Nottingham et al., 2001; Ritucci et al., 2005), the medullary raphe (Bouyer et al., 2004), and the LC (Filosa et al., 2002; Hartzler et al., 2008). Additionally, hypercapnia-induced pH_i recovery is also absent in other CO_2/H^+ sensing cells, such as chemosensitive neurons from invertebrate preparations (Goldstein et al., 2000), peripheral chemosensitive glomus cells (Buckler et al. 1991a; 1991b), adrenal chromaffin cells from neonatal rats (Muñoz-Cabello et al., 2005), and the sour-sensing taste bud receptors (DeSimone et al., 2001). Thus, a lack of pH_i recovery in the face of an acid challenge (both intra- and extracellular) appears to be a common feature of all CO_2/H^+-sensitive cells.

One might expect that neurons from chemosensitive regions, as they use a change of pH_i as a signal, would have lower intercellular buffering power than neurons from non-chemosensitive regions since this would magnify the pH_i change in response to an acid stimulus. However, high values of intrinsic buffering (approx. 46 mM/pH unit) have been measured in neurons from both chemosensitive and nonchemosensitive regions of the neonatal rat brainstem (Ritucci et al., 1998; Chambers-Kersh et al., 2000). It was

proposed that the high buffering power could be construed as a form of cellular protection against prolonged acidic conditions (Ritucci et al., 1998). Whatever the case, these findings ultimately indicate that differences in intrinsic buffering power do not appear to play a part in the determination of a chemosensitive neuron.

As discussed above, pH-regulating membrane transporters appear to be present in all cells (Putnam and Roos, 1997) including brainstem neurons (Putnam, 2001). The pH inside a cell is regulated by numerous membrane transporters, including at least seven isoforms of Na^+/H^+ exchangers (NHE) (Orlowski and Grinstein, 2004), and a variety of HCO_3-dependent transporters, including Na^+-HCO_3^- cotransporters (NBC), and by Na^+-dependent (NDCBE) and Na^+-independent (AE) forms of Cl^-/HCO_3^- exchangers (Putnam 2001; Chesler 2003; Romero et al., 2004; Nicola et al., 2008)

NHE's are present in almost all cells and contribute to alkalinizing pH recovery from acid loads (Counillon and Pouysségur, 2000; Orlowski and Grinstein, 2004), extruding H^+ in exchange for the entry of Na^+ and resulting in a return towards the cell's initial pH_i value. It is believed that this is the dominant protein for pH_i recovery in brainstem neurons (Ritucci et al., 1997, 1998; Nottingham et al., 2001, Wiemann and Bingmann, 2001). There is debate about exactly which isoform of NHE is present in neurons from various chemosensitive regions. Kersh et al. (2009), using isoform specific inhibitors, found that NHE1 is predominant in NTS and ventrolateral medulla neurons, although there is some evidence for a minor role played by NHE3. In contrast, Kiwull-Schöne et al. (2001) argued that NHE3 is the predominant isoform since inhibition of this isoform seems to alter pH_i in certain ventral medullary neurons and to reduce the ventilatory response to inspired CO_2. There is also the suggestion that NHE5 may be

common in rat brainstem neurons (Kersh et al., 2009) but no specific inhibitor exists for this isoform.

Sodium-driven Cl^-/HCO_3^- exchangers mediate a cell's alkalinizing intracellular pH recovery from acid loads by exchanging a Na^+ from outside the cell for an internal Cl^- with two acid equivalents removed from inside (Putnam and Roos, 1997; Putnam, 2001). NDCBE has been identified in the hippocampus in both freshly dissociated and cultured neurons (Bevensee et al., 1996), as well as cerebellar granular neurons (Pocock and Richards, 1992). Active NDCBE has not been demonstrated in brainstem neurons. This transporter is similar to NBC cotransporters, which transport 1 Na^+ for 1-3 HCO_3^- ions, but do not involve Cl^- transport (Romero et al., 2004). NBC cotransporters have been shown to play some role in pH_i recovery in rat brain endothelial cells (Taylor et al., 2006; Nicola et al., 2008), but have yet to be shown as functionally active in neurons from chemosensitive regions. However, recent evidence suggests that an electroneutral form of NBC, NBCn1, may play a major role in pH_i recovery from an acid load in LC neurons (Kersh et al., 2009).

It is currently unknown what advantages a neuron might have by containing a particular transporter or combination of transporters. Regardless, it is remarkable that despite the specific pH-regulating transporters present on neurons from various chemosensitive cells, pH recovery from acidosis is inhibited in response to hypercapnic acidosis in all of these neurons.

Methods for pH_i Measurement

In vitro studies measuring pH_i have used several different preparations, including freshly dissociated neurons (Raley-Susman et al., 1993, Schwiening and Boron, 1994;

Bevensee et al., 1996; Smith et al., 1998, Nicola et al., 2008), cell cultures (Baxter and Church, 1996; Church et al., 1998, Diarra et al., 1999; Wang and Richerson, 2000; Taylor 2006), and explant cultures (Wiemann and Bingmann, 2001). Most studies of chemosensitive neurons, though, have been done in brain slices (Cowan and Martin, 1995; Ritucci et al., 1996; Trapp et al., 1996; Filosa et al., 2002; Hartzler et al., 2008; Nichols et al., 2008; Conrad et al., 2009), which also have been used for this work. Two main techniques have thus far been used to measure pH_i, with variations and advancements evolving over the years as dependent on the preparations mentioned above.

Microelectrodes

The use of pH-sensitive microelectrodes for intracellular pH measurement extends back several years, involving the use of either pH-sensitive glass or a double-barreled liquid-ion exchange (LIX) electrode. However, pH-sensitive electrodes can be damaging to the neuron they impale, and thus were more primarily utilized for larger cells such as snail and other invertebrate neurons (Boron and De Weer, 1976; Thomas 1974). Later on, smaller-tipped LIX electrodes were constructed and used to study cat respiratory neurons (Ballanyi et al., 1994), dorsal vagal rat motoneurons (Cowan and Martin, 1995), and rat thigh muscle cells (Khuri et al., 1992). Still, they are not as popularly used today as pH-sensitive fluorescent dyes which, in contrast, have a number of advantages described next.

Fluorescent dyes

pH-sensitive fluorescent dyes have numerous advantages over the use of pH-sensitive microelectrodes. They can be used to study smaller neurons and cells, used to study several cells within a preparation at the same time, used to study pH_i in different

parts of a cell with fluorescence imaging microscopy, and can provide high resolution of pH_i change both spatially and temporally (Grinstein and Putnam, 1994; Ritucci et al., 1996). A large host of pH-sensitive dyes exist, but commonly used dyes for studying neurons include pyranine (Mulkey et al., 2004; Nichols et al., 2009), and 2',7'-bis(carboxyethyl)-5(6)-carboxyfluorescein (BCECF) (Bevensee et al., 1995; Ritucci et al., 1996; Filosa and Putnam, 2002; Schewe et al., 2008), the latter of which is said to be the most commonly used (Putnam et al., 2001).

Each pH-sensitive dye has its own advantages and disadvantages. For example, pyranine is both inexpensive and causes less damage to the cell compared to BCECF, and it exhibits minimal photobleaching (Gan et al., 1998). However, it is highly impermeable to the cell membrane and requires manual injection, usually employing whole patch pipettes. Such loading of pyranine results in the loading of but a single cell with pH-sensitive dye. BCECF, on the other hand, can be readily loaded into most cells by incubating cell cultures or slices with the membrane permeant form of BCECF, using its acetyoxyl methyl ester form (BCECF-AM) (e.g. Ritucci et al., 1996). The dye enters the cell and the AM groups are cleaved rendering the BCECF portion fluorescent and trapped within the cell (Ritucci et al., 1996; Putnam, 2001). However, the cleaved AM group forms formaldehyde which can be damaging to the cell. Further, BCECF does have some leakage from the cell and does exhibit photobleaching so the length of an experiment may be limited by these factors. In a variant on these techniques, BCECF has been loaded into a single neuron by placing BCECF-AM into the barrel of a perforated patch pipette (Filosa et al., 2002). Under such conditions, the cell membrane is not broken, but only small holes made in the membrane by the perforating agent, Amphotericin B.

Amphotericin B is an ionophore that, when added to the pipette filling solution, makes contact with the portion of the cell membrane that is patched and renders it permeable without rupturing it. This allows for the diffusion of substances between the pipette and cell interior, including membrane permeable dyes. The BCECF-AM in the pipette can diffuse across the patch and load the patched neuron, where the AM group is cleaved as usual and the patched cell becomes loaded with the pH-sensitive fluorescent form BCECF. Similar techniques have been used with either perforated or whole cell patch electrodes to make simultaneous measurements of V_m and pH_i (Trapp et al., 1996, Ritucci et al., 1998, Hartzler et al., 2008; Nichols et al., 2008). Nevertheless, both pyranine and BCECF have been used with great effectiveness to study the response of pH_i within chemosensitive neurons.

Methods of pH_i Clamping

As previously mentioned, more research needs to be done to clarify the role of pH_i in the chemosensitive response. The best way to test this would be to keep pH_i constant, in other words "clamp" pH_i, and manipulate the other potential signals, pH_o and CO_2, with pH_i clamped.

A technique to clamp pH_i has previously been described (Grinstein et al., 1994). In this technique, macrophages were patched (either with whole cell or perforated patch pipettes) and a sizeable pool of a weak base (NH_4^+) was loaded into the cytoplasm from the pipette. By varying the external concentration of NH_4^+ pH_i could be set at any value desired based on the Henderson-Hasselbalch equation. This technique was adapted for clamping pH_i in chemosensitive neurons. In response to a hypercapnic acid challenge, the plan was to increase extracellular NH_4^+ to generate a counterbalancing influx of base.

However, it was found that elevating extracellular NH_4^+ resulted in a marked membrane depolarization and loss of firing due to depolarization block (Hartzler et al., 2008). This finding was interpreted as external NH_4^+ functioning like elevated K^+, and resulted in depolarization. Hartzler et al. (2008) modified this technique by using the whole cell patch pipette to load the neuron with weak acid (acetic acid) rather than weak base. Now upon exposure of the neuron to a hypercapnic acid solution, extracellular acetate was lowered creating a counterbalancing weak acid efflux (Figure 6). Further, this adaptation of Grinstein's original technique also allows for pH_i to be clamped at any value. Thus, in the same neuron, upon exposure to an acid challenge we can either allow pH_i to decrease or to remain the same. Therefore each neuron can serve as its own control. In this thesis, I looked to extend the ability to clamp pH_i in the face of acid challenges in chemosensitive neurons using modifications of these existing techniques.

FIGURE 6. Drawing of weak-acid diffusion chemistry for blunting pH_i. Blue arrows indicate diffusion. A weak acid (e.g. acetic acid), HA_i, is loaded into the cell either through a patch pipette directly or through membrane diffusion. Then, in the presence of hypercapnia, CO_2 diffuses through the membrane and acidifies the cell through the reaction catalyzed by carbonic anhydrase (CA). At the same time, the concentration of the weak acid (e.g. acetic acid) is lowered outside the cell, HA_o. This forms a concentration gradient with previously loaded HA_i and allows for the passive diffusion of HA outside the cell. As HA flows out, this drives the weak-acid dissociation reaction to the left (as shown) and consumes internal H^+. Thus weak acid efflux counterbalances the acidification normally seen by the introduction of CO_2, resulting in a clamping of pH_i.

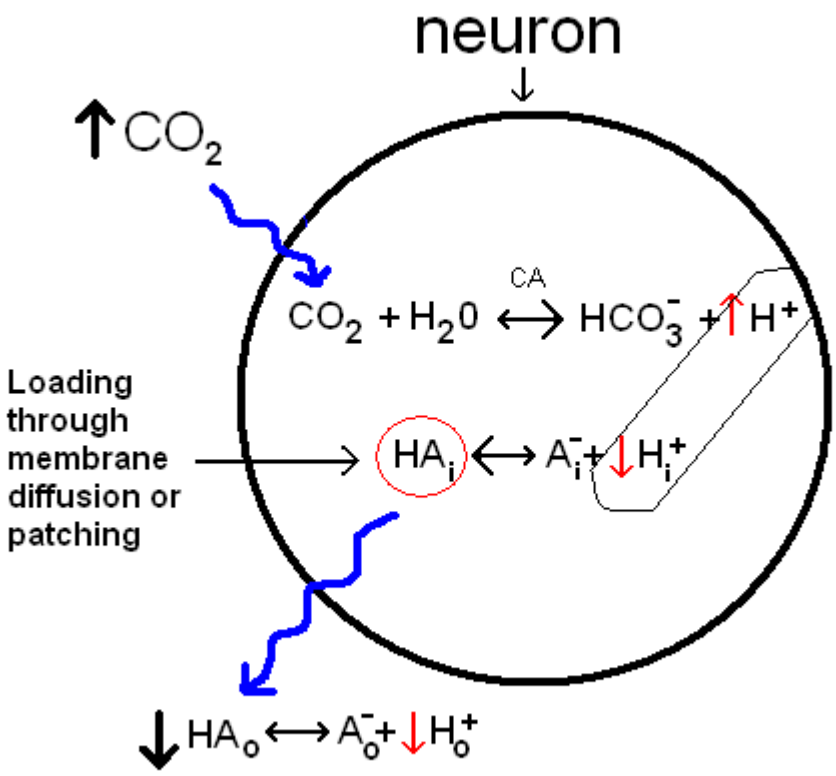
neuron
$\uparrow CO_2$
CA
$CO_2 + H_20 \leftrightarrow HCO_3^- + \uparrow H^+$
Loading through membrane diffusion or patching
$HA_i \leftrightarrow A_i^- + \downarrow H_i^+$
$\downarrow HA_o \leftrightarrow A_o^- + \downarrow H_o^+$

CHAPTER III

HYPOTHESIS & AND SPECIFIC AIMS

This research project is designed to develop new techniques to clamp intracellular pH in the face of an acid challenge. These techniques focus on those neurons believed to be involved in central respiratory control in order to allow us to ultimately study the involvement of changes of pH_i in chemosensitive signaling, but may have greater applicability for studying the role of pH_i in a variety of functions in other cells as well. **Our hypothesis is that we can to clamp pH_i in the face of acid challenges either by substantially increasing intracellular buffering power or by creating a counter-balancing efflux of weak acid.**

Specific Aims

The proposed work is divided into two specific aims:

Specific Aim 1: Attempt to minimize changes of intracellular pH in response to hypercapnic acidosis (15% CO_2, pH_o ~7.0 from control values of 5% CO_2, pH_o ~7.45) in neurons from chemosensitive brainstem regions by increasing their intracellular buffering power. Blunting will be achieved through the use of whole cell patching of individual neurons within a brainstem slice using patch pipettes that contain either high or low concentrations of buffer.

Specific Aim 2: Attempt to clamp intracellular pH in the face of hypercapnic acidosis in neurons from chemosensitive brainstem regions by inducing a counter-balancing efflux of weak acid or a concurrent influx of weak base.

Aim 2a: Neurons will first be loaded with high concentrations of a weak acid (with weak acid maintained extracellularly) and then exposed to hypercapnic acidosis with extracellular weak acid at a high concentration (no supposed pH_i clamping) or at a low extracellular weak acid concentration (presumptive pH_i clamping).

Aim 2b: Simultaneously expose neurons to hypercapnic acidosis and a weak base with the intent to clamp pH_i with a base influx comparable to the acid influx.

In Aim 2, clamping should be present in all the cells of the slice, not just in a single patched neuron as in Aim 1.

In all experiments, brainstem slices will be studied from neonatal rats and neurons will be visualized from two putative chemosensitive regions, the NTS and the LC.

CHAPTER IV

MATERIALS AND METHODS

Slice Preparation

LC and NTS slices were taken from the brainstem of postnatal (P) Sprague-Dawley rats ages P3 to P17 as previously described (Ritucci et al., 1996; Ritucci et al., 1997; Ritucci et al., 2005; Filosa et al., 2002; Conrad et al., 2009). Hypothermic anesthetization (-18^{o}C for ≤ five minutes) was used for rats ages P3 to P9 prior to rapid decapitation with 6 inch scissors (World Precision Instruments). CO_2 anesthetization (100% CO_2 for ~1-2 minutes) was used for rats ages P10-P17 prior to rapid decapitation with a guillotine (Scientific Equipment Inc.). A tissue segment ranging from the mid-pons to the upper cervical spinal cord was then dissected in 5% CO_2 / 95% O_2-bubbled artificial cerebral spinal fluid (see below for recipe) and further cut with a vibratome (Pelco 101 Vibratome 1000) into 300μm thick transverse slices (Figure 7). Slicing was done in the rostral direction starting with the spinal cord at 4-6^{o}C and also in 5% CO_2 / 95% O_2-bubbled artificial cerebral spinal fluid (aCSF). Finished slices were then incubated at room temperature in 5% CO_2 / 95% O_2-bubbled aCSF (pH ~ 7.45) for 15 minutes to allow recovery from the slicing process. All procedures involving animals were approved by the Institutional Animal Care and Use Committee at Wright State University.

Solutions

The aCSF solution was comprised of (in mM) 124 NaCl, 26 $NaHCO_3$, 5 KCl, 1.24 KH_2PO_4, 10 glucose, 1.3 $MgSO_4 – 7H_20$, and 2.4 $CaCl_2$. Synaptic block aCSF (SNB) contained 117 NaCl, 26 $NaHCO_3$, 5 KCl, 1.24 KH_2PO_4, 10 glucose, 11.4 $MgSO_4 – 7H_20$, and 0.2 $CaCl_2$ (Huang et al., 1997).

The 45.5mM Na-acetate solution (high Na-ace) contained 78.5 NaCl, 5 KCl, 1.24

FIGURE 7. Dorsal view of the neonatal rat brainstem, with the rostral end facing the top of the page. The cerebellum is cut away showing the locations of the NTS and LC regions in the medulla and pons, respectively. A drawing of transverse tissue slices (~300μM thick) is to the right, indicating the NTS (green) and LC (red) regions within each. Both regions are located in the dorsal part of the slice.

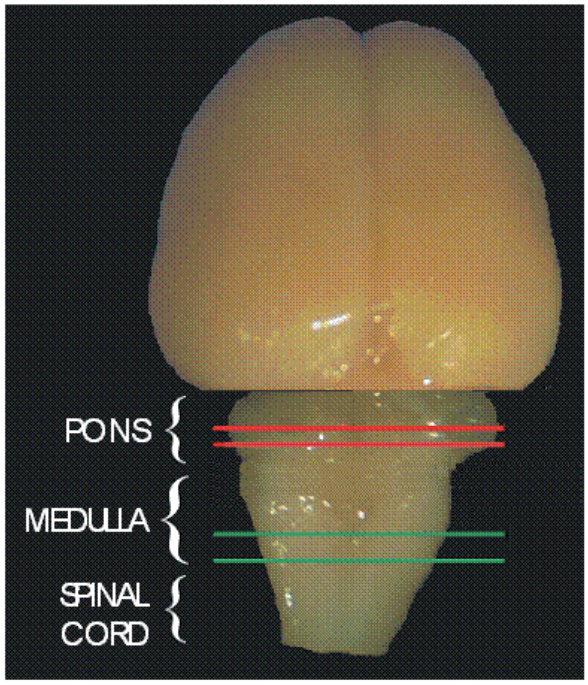
PONS
MEDULLA
SPINAL
CORD

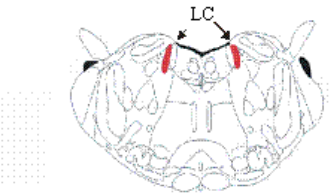
LC

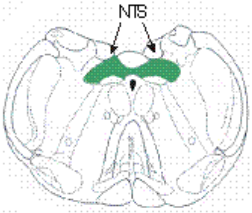
NTS

KH_2PO_4, 10 glucose, 1.3 $MgSO_4 – 7H_20$, 2.4 $CaCl_2$, 45.5 $NaCH_3COO$, and pH was adjusted to 7.45 by slowly adding $NaHCO_3$ while bubbling with 5% CO_2 / 95% O_2. The 16.16mM Na-acetate solution (low Na-ace) was prepared the same as the high Na-ace solution but iso-osmotically recalculated with (in mM) 107.84 NaCl and 16.16 $NaCH_3COO$.

The 45.5mM Na-caproate solution (high Na-cap) contained 78.5 NaCl, 5 KCl, 1.24 KH_2PO_4, 10 glucose, 1.3 $MgSO_4 – 7H_20$, 2.4 $CaCl_2$, 45.5 $CH_3(CH_2)_4COONa$, and pH adjusted to 7.45 by slowly adding $NaHCO_3$ while bubbling with 5% CO_2 / 95% O_2. The 16.16mM Na-caproate solution (low Na-cap) was prepared the same as the high Na-cap solution but iso-osmotically recalculated with (in mM) 107.84 NaCl and 16.16 $CH_3(CH_2)_4COONa$ instead.

The trimethylamine (TMA) solution contained (in mM) 99 NaCl, 5 KCl, 1.24 KH_2PO_4, 10 glucose, 1.3 $MgSO_4 – 7H20$, 2.4 $CaCl_2$, 25 TMA, and pH was adjusted to 7.45 by slowly adding $NaHCO_3$.

The pH of all solutions was determined with an ORION microprocessor pH/millivolt meter (model 811) while bubbling with 5% CO_2 / 95% O_2 at 37^oC. All chemicals were purchased from EMD Chemicals Inc., Sigma, and Fischer Scientific. All solutions were newly made with the pH adjusted each day.

Pipette Filling Solutions

Low HEPES whole cell patch pipette intracellular solution was comprised of (in mM) 130 K^+-gluconate, 10 KCl, 0.4 EGTA, 1 $MgCl_2$-$6H_2O$, 0.3 GTP, 2 ATP, and 10 HEPES. High HEPES whole cell pipette solution was comprised of (in mM) 40 K^+-gluconate, 10 KCl, 0.4 EGTA, 1 $MgCl_2$-$6H_2O$, 0.3 GTP, 2 ATP, and 100 HEPES. The

pH of both solutions were adjusted to ~ 7.45 at room temperature with KOH. The solutions were pipetted in 1 mL amounts into microcentrifuge tubes and stored in the freezer until use.

Dye-Loading

Two types of pH-sensitive fluorescent dyes and two forms of dye-loading were used. The membrane-impermeable dye pyranine was used and loaded directly into the cell using whole cell patching (see Whole Cell Methods below). A membrane permeable form of the dye, 2',7'-bis-(2-carboxyethyl)-5-(and-6)-carboxyfluorescein (BCECF), BCECF-acetoxymethyl ester (BCECF-AM) (B-1150 Invitrogen Molecular Probes), was also used and was loaded through membrane diffusion. Once loaded, the acetoxymethyl ester (AM) groups were cleaved by intracellular esterases to form the membrane impermeable BCECF.

For the diffusion process, slices containing the NTS and LC regions were transferred to a dish containing 5mL of 20μM of BCECF-AM in aCSF (equilibrated with 5% CO_2 / 95% O_2 gas at 37^{o}C) and incubated for 30 minutes in total darkness. They were then washed in 5% CO_2 / 95% O_2 equilibrated aCSF for at least 30 minutes at room temperature until ready for imaging and remained in darkness throughout.

Whole Cell Methods

Pipettes (TW150-3 World Precision Instruments) were made of thin wall borosilicate glass (1.5 / 1.12 OD/ID) and pulled to a 5 MΩ tip resistance. The pH-sensitive pyranine dye (200μM of a 4mM stock) was added to the pipette filling solution (see above) in darkness before filling the tip. Pipettes were held and maneuvered into place by a Narishige MX-2 micromanipulator. Positive pressure was applied to the

pipette to prevent obstruction and clear debris from the surface of a neuron before obtaining a gigaseal using slight negative pressure once the tip touched the cell. Manual suction was then used to break the membrane. Patching was done using a Dagan BVC-700 amplifier and Grass S48 stimulator in current clamp mode, visualizing cells through a monitor (SONY) connected to a video camera (Dage model MTI CCD 72). Action potentials (APs) were visualized through a Tetronix TDS 1012B Oscilloscope and integrated (10 second bins) with a slope/height window discriminator (FHC). APs were also confirmed by popping sounds using a Grass AM8 Audio Monitor.

Setups and Chamber Conditions

Two imaging microscopes, one an upright microscope and the other an inverted microscope, were used for the studies of pH_i. Dye-loaded slices were placed in a Plexiglas superperfusion chamber with a glass cover slip bottom (~ 180 μm thick) on the stage of each microscope. During the experiments, slices were held in place with nylon fibers attached to a platinum wire frame. Glass jars containing the solutions were maintained at 37^{o}C within a water bath and equilibrated with gas as follows: normocapnic aCSF, SNB, high Na-ace, and high Na-cap solutions were equilibrated with 5% CO_2 / 95% O_2, pH ~ 7.45 at 37^{o}C. Hypercapnic aCSF, SNB, high Na-ace, low Na-ace, high Na-cap, low Na-cap, and TMA solutions were equilibrated with 15% CO_2 / 85% O_2, pH ~ 7.0 at 37^{o}C.

Inverted Setup

Some experiments used a Nikon Eclipse T*i*-S inverted microscope. Solutions were gravity fed first through stainless steel tubing (1.6 / 0.5mm OD/ID), a glass bubble trap, a thermoelectric Peltier assembly, through the perfusion chamber, then lastly

removed with a vacuum trap to allow for the fresh, continuous flow of solution (3.5-4 ml/min). The chamber itself was maintained at a temperature of approx. 37^{o}C, held in near-constant darkness, and covered with a glass cover slip resting on the top surface of the Plexiglas stage to maintain constant solution flow and depth.

Upright Setup

Upright experiments employed a Nikon Eclipse E600 microscope. Solutions were also fed through the same assembly described above, at a rate of flow of about 3-5 ml/min. The chamber itself was maintained at 36 ±1^{o}C in the dark, but not covered with a glass cover slip.

pH Imaging

pH_i was measured as previously described (Rittuci et al., 1996; Rittuci et al., 2005) with fluorescence imaging microscopy. All pH measurements were recorded from the cell soma.

Imaging with Patching

While patching, only one cell was visualized at a time. Cells were visualized (total magnification approx. 720X) using the upright microscope with a 60X water-immersion objective (NA 0.8, 3.0 mm working distance). A single cell was loaded with pyranine from a patch pipette for three-five minutes and confirmed by viewing the fluorescent cell body using Metafluor software (version 7.1.3.0, Molecular Devices) (Figure 8). A xenon lamp and Sutter Lambda 10-2 filter wheel were used to alternately excite the pyranine-loaded cell with 415 and 450 nm light, and the emitted fluorescence (515nm) was recorded with a CCD 72 camera and GenIIsys image intensifier (Dage-MTI). Each image was collected over 99 milliseconds and new images were collected at

FIGURE 8. Pyranine-loaded NTS cell using the whole cell method. The faint body of the pipette tip is also shown approaching from the lower-left.

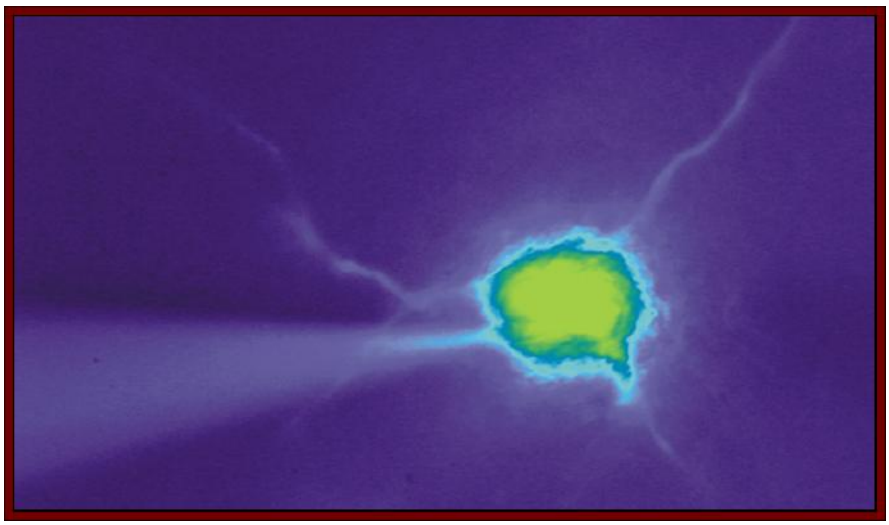

60 second intervals and collected using Metafluor software on an HP Compaq computer.

Imaging without Patching

Without patching, multiple neurons in a slice could be visualized at once during the experiment. BCECF-loaded LC and NTS neurons were imaged on both the upright and inverted setups. pH_i was recorded on the upright microscope as above but with 198 millisecond images. Cells on the inverted microscope were visualized with a 40X objective, with more than one cell able to be visualized at once (Figures 9 and 10). Emitted fluorescence (525nm) was recorded with a CoolSnap HQ^2 camera (Photometrics) after excitation of the cell with 440 and 495 nm light for BCECF loaded cells.

Data Analysis

Data analysis was conducted using Excel (Microsoft Office 2003). pH_i was determined by taking the fluorescence ratios (R_{fl}) from Metaflour (440/480 for BCECF-AM and 415/450 for pyranine) and normalizing them to controls (N_{fl}) specific for each brainstem region. Values of pH_i were calculated and then graphed vs. time from the following calibration equations: $pH_i = 7.5561 + \log(N_{fl} – 0.1459)/(2.0798 - N_{fl})$ for LC cells (Ritucci et al., 2005), and $pH_i = 7.272 + \log(N_{fl} – 0.0841)/(1.9725 - N_{fl})$ for NTS cells (Ritucci et al., 1997). Percent blunting averages were calculated as described in the Results section.

Statistics

Kyplot versions 3.0 and 2.0 beta 15 were used for all statistical calculations. The means, standard errors, and changes in pH_i between the LC and NTS regions and between superfusate solutions were calculated and compared using unpaired parametric t-tests. For all tests, a value of $P<0.05$ was considered statistically significant, a value of

FIGURE 9. BCECF-AM loaded slice viewing the NTS region using the weak acid diffusion method. Bright fluorescent ovals are NTS cell somas.

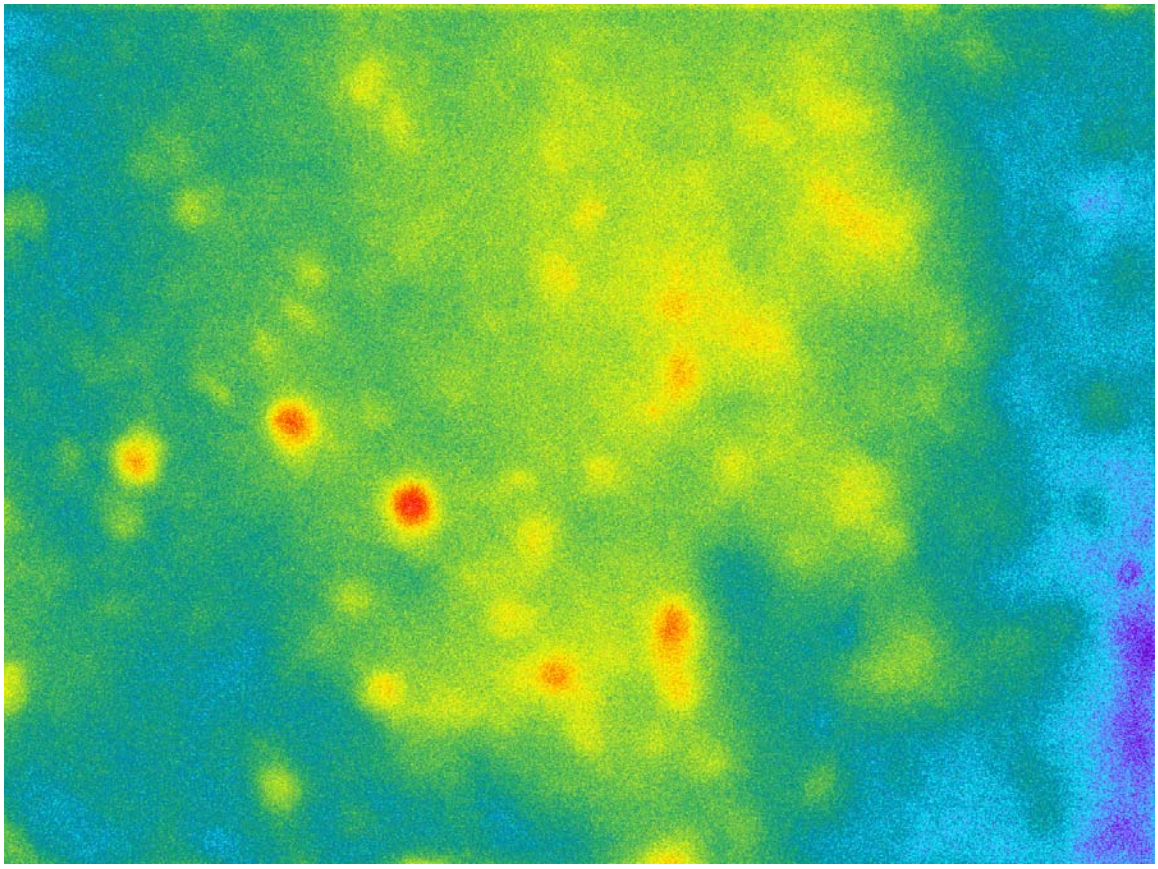

FIGURE 10. BCECF-AM loaded slice viewing the LC region using the weak acid diffusion method. Bright fluorescent ovals are LC cell somas. Note that the ovals are bigger than the cells in Figure 9, as LC neurons are larger.

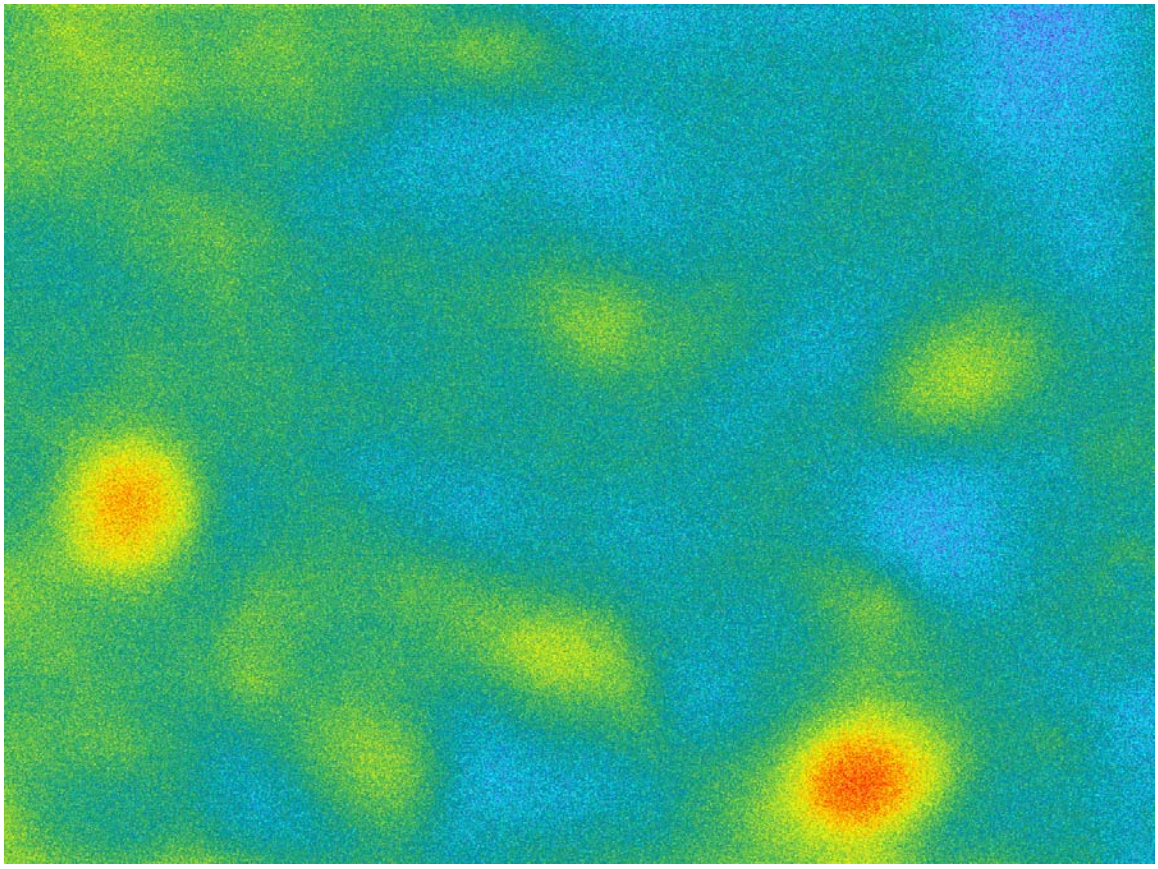

$P<0.01$ was considered highly significant, and a value of $P<0.001$ was considered very highly significant.

CHAPTER V

RESULTS

In this work, we experimented with different ways to clamp intracellular pH: first via buffering using whole cell patch pipettes in individual neurons within brainstem slices, second via the simultaneous introduction of weak base in the presence of HA, and third by adapting the weak-acid diffusion method (see below) in whole slices. Blunting results are given in blunting percentages or "percent blunting", which is expressed as:

% blunting = 100 x (1- (ΔpH_i under experimental conditions)/(ΔpH_i under control conditions))

where ΔpH_i is the decrease in pH_i induced by hypercapnia. A higher % blunting indicates better pH_i clamping upon exposure to hypercapnia, with a value of 100% indicating no change of pH_i upon exposure to hypercapnia. All pH_i mean values are rounded to two decimal places, and standard error to three.

Effect of HEPES Buffer in the NTS using Whole Cell Patch Clamp Technique

We first attempted to blunt ΔpH_i in response to hypercapnia by using an increased concentration of HEPES buffer (100mM) in the whole cell patch pipette in individual NTS neurons within brainstem slices. We patched 55 neurons, 27 of which were patched with pipettes containing high HEPES (100 mM) and 28 patched with pipettes containing normal HEPES (10 mM). The slice was superfused with aCSF designed for synaptic blockade (SNB: ↑Mg, ↓Ca) and equilibrated with 5% CO_2 (pH_o ~7.45). Neurons were then exposed to the same solution equilibrated with 15% CO_2 (pH_o ~7.0) and the magnitude of hypercapnia-induced acidification was measured. Sample traces are shown in Figure 11. In Figure. 11A (low HEPES) we see that hypercapnia induces a reversible acidification of about 0.1 pH unit. In contrast, the use of high HEPES largely reduced the acidification induced by hypercapnia (Figure 11B). The averages of these experiments are shown in Fig. 12. In low HEPES, hypercapnia resulted in an acidification of 0.12 ±

FIGURE 11: Effect of hypercapnia on pH_i in NTS neurons patched with whole cell pipettes containing either low HEPES **(A)** or high HEPES **(B)**. **A:** Individual trace of pH_i vs. time in an NTS neuron patched with a whole cell pipette that contains low (10 mM) HEPES buffer. Note that two exposures to hypercapnia (15% CO_2) each resulted in a substantial and similar acidification. **B:** Individual trace of pH_i vs. time in an NTS neuron patched with a whole cell pipette that contained high (100 mM) HEPES buffer. Note that in the presence of high HEPES in the pipette, hypercapnia-induced acidification was substantially smaller.

A.

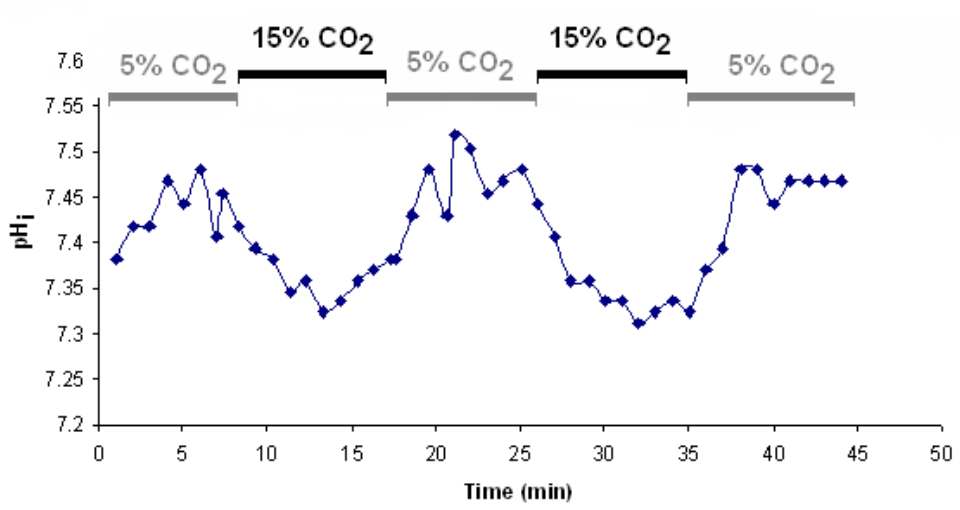
15% CO2
5% CO2
15% CO2
5% CO2
7.6
7.55
7.5
7.45
7.4
7.35
7.3
7.25
7.2
pHi
0
5
10
15
20
25
30
35
40
45
50
Time (min)

B.

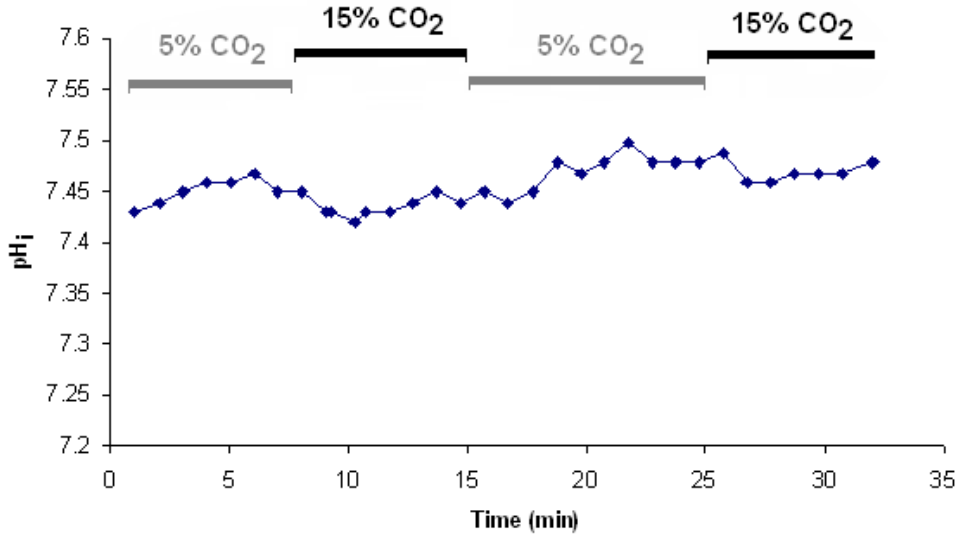
15% CO2
5% CO2
5% CO2
15% CO2
7.6
7.55
7.5
7.45
7.4
7.35
7.3
7.25
7.2
pHi
0
5
10
15
20
25
30
35
Time (min)

FIGURE 12. Bar graph showing average hypercapnia-induced ΔpH_i in NTS neurons patched with pipettes containing low or high HEPES. The height of a bar indicates the mean ΔpH_i and the error bars represent 1 SEM. The number of neurons is indicated inside each bar and *** indicates the average values are very highly significantly different ($P<0.001$).

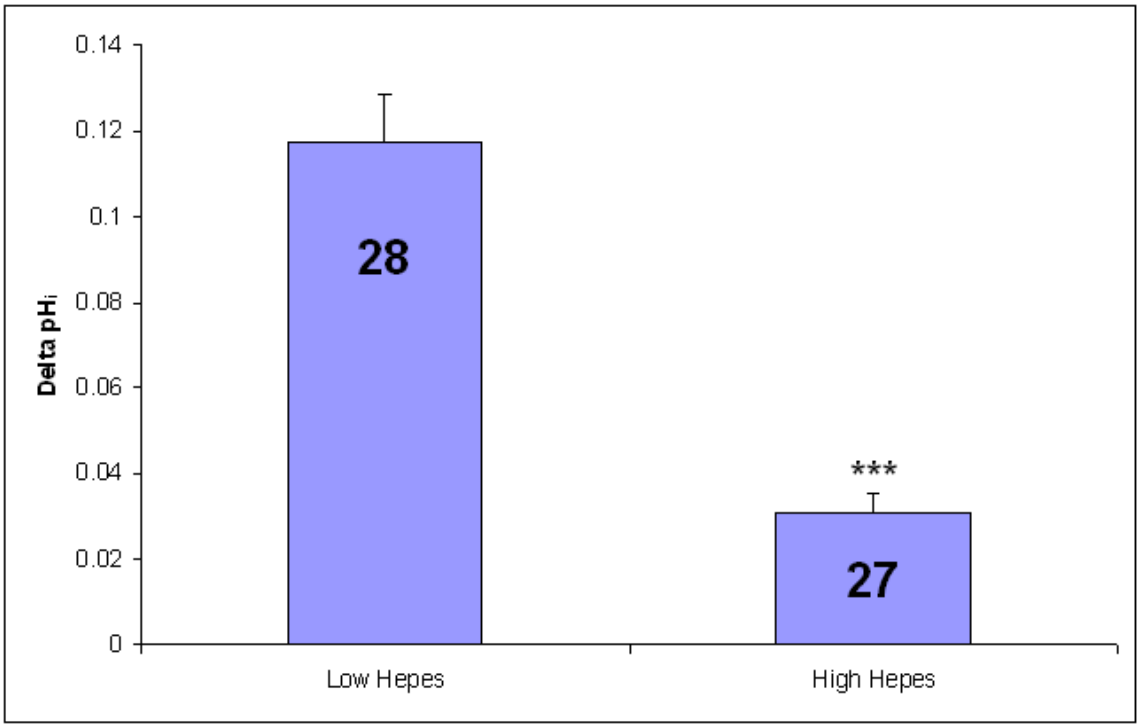
0.14
0.12
0.1
0.08
0.06
0.04
0.02
0
Delta pHi
28
***
27
Low Hepes
High Hepes

0.011 pH unit while the acidification was only 0.03 ± 0.004 pH unit in high HEPES. These differences were very highly significantly different ($P<0.001$) with a calculated % blunting of 73.4%.

As already mentioned, HEPES experiments were performed with synaptic blockade medium (SNB). This was due to our efforts to simultaneously make electrophysiological recordings in conjunction with pH_i measurements, and we used SNB to block any potential contributions from chemical synapses to the firing rate of NTS neurons (Dean et al., 1990; Conrad et al., 2009). It proved difficult to maintain a prolonged patch in NTS neurons to obtain good firing rates. However, a single successful electrophysiological recording of an NTS neuron with a whole cell patch containing low HEPES is shown in Figure 13A. The corresponding simultaneous pH trace is shown below it in Figure 13B. Note that hypercapnia induces a substantial decrease of pH_i and a large, reversible increase in firing rate in this NTS neuron. Nonetheless, whole cell patching of NTS neurons proved to be a very challenging technique and was capable of blunting pH changes in only one neuron at a time. We therefore looked to develop other ways of blunting hypercapnia-induced pH_i changes.

Weak Acid Diffusion

The weak-acid diffusion method was adapted from Hartzler et al. (2008) which in turn was adapted from the rapid diffusion of weak bases technique devised by Grinstein et al. (1994). In this technique, intracellular pH levels are maintained (clamped) upon exposure to hypercapnia by introducing high concentrations of weak acid to the cell interior using whole cell patch pipettes containing the weak acid. Then, upon exposure to hypercapnia, a lowering of the weak acid concentration outside occurs to promote

FIGURE 13: An electrophysiological recording from an NTS neuron from a neonatal rat with whole cell patch pipette containing low (10 mM) HEPES buffer **(A)** with its corresponding pH_i trace **(B)**. **A:** Electrophysiological recording using the whole cell patch technique. The bottom panel shows the membrane potential vs. time, with upward deflections showing individual action potentials. The upper panel shows the integrated firing rate (10 s bins) reported in impulses/s (Hz). Note that in response to two hypercapnic challenges, the firing rate increased reversibly. **B:** Individual trace of pH_i vs. time in the same patched NTS neuron. Note that the two exposures to hypercapnia (15% CO_2) each resulted in a substantial and similar acidification.

A.

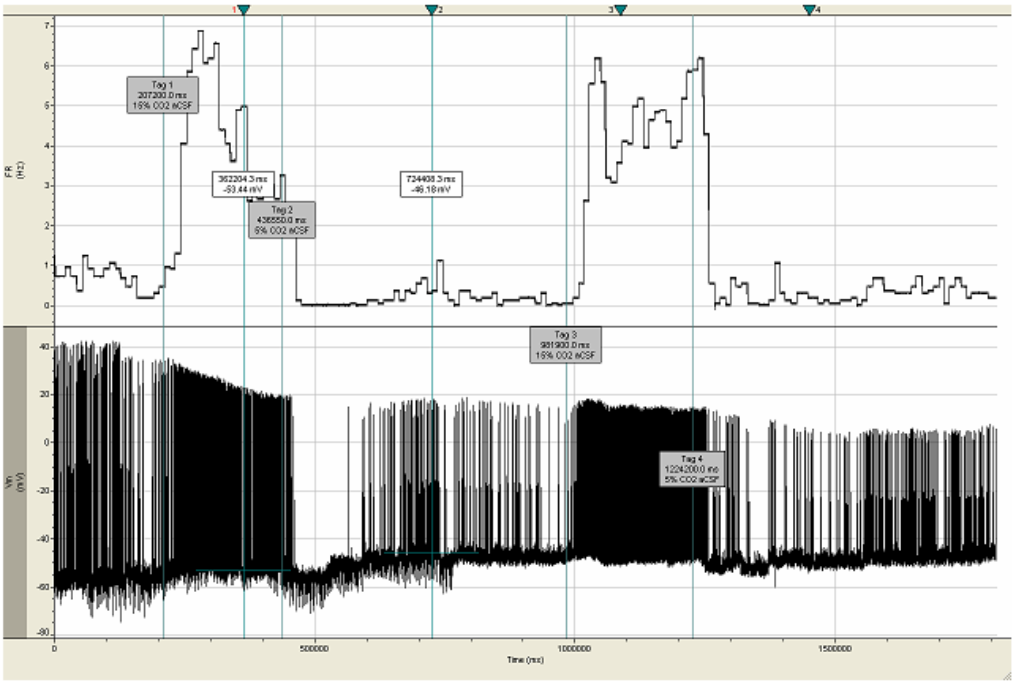
Tag 1
Tag 2
Tag 3
Tag 4
FR (Hz)
Vm (mV)
Time (ms)

B.

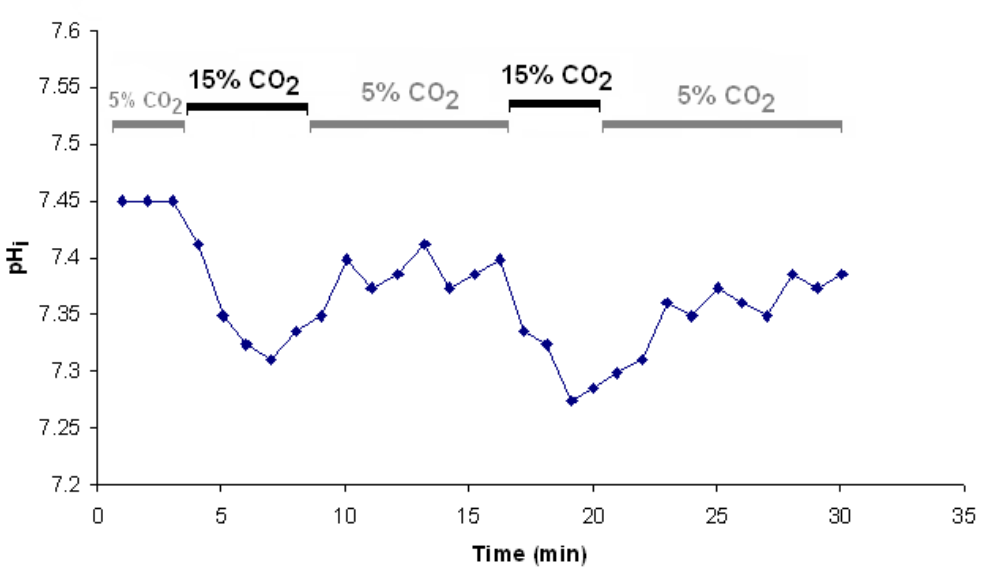
5% CO2
15% CO2
5% CO2
15% CO2
5% CO2
pHi
Time (min)

diffusion of the weak acid out of the cell, creating a counterbalancing H^+ efflux which neutralizes the hypercapnia-induced H^+ influx. In this way, one can potentially keep intracellular pH constant (see Figure 6 for diagram of this process).

Initial Acidification Due to Weak Acid Loading

Because whole cell patching can blunt pH changes only in one cell at a time, we were interested in other methods to see if pH_i blunting could be achieved in multiple cells at once. We thus applied the weak-acid diffusion principle to whole slices. However, this required loading the cells with initial amounts of acid through means other than the patch pipette. We were able to load the cells instead by exposing the slice to a high concentration of the experimental acid in normocapnia (5% CO_2), allowing it to diffuse across the cells' membranes. This way, one can potentially clamp pH_i both without the need for patching as well as in the entire slice.

Exposing a cell to high acid concentrations under normocapnic (5% CO_2) conditions for at least 20 minutes resulted in an acidification. This acidification validated that acid was being loaded into the cells. Figure 14 shows this initial acidification, indicated by the red circles, in two traces of NTS neurons using 45.5mM Na-acetate solution equilibrated with 5% CO_2. This acidification ranged from 0.01 to 0.18 pH unit across all acid-loading (Na-acetate and Na-caproate) experiments. In response to this weak-acid induced acidification, cells in both the NTS and LC regions either remained acidified following the initial drop in pH_i (upper trace in Figure 14) or underwent partial pH_i recovery (lower trace in Figure 14), with observed variation in the levels of recovery. In either case, it was from this ending pH value that subsequent changes in pH_i were calculated. With patching, weak acid is loaded directly into the neuron at the same pH

FIGURE 14: Two example traces of pH_i vs. time in two separate NTS neurons showing initial acidification (circled in red) from normocapnic, high concentration Na-acetate solution. The top graph shows no pH_i recovery while the bottom graph shows pH_i recovery. Traces are from individual cells in the NTS region and also from different slices. However, neurons recovering or not recovering from the initial pH drop could vary in their recovery response within the same slice.

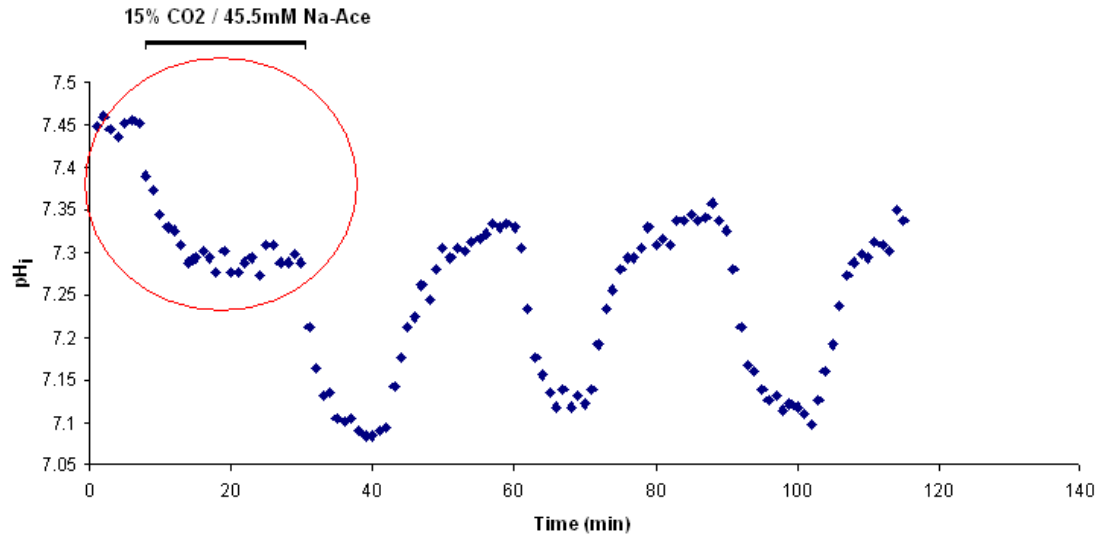
15% CO2 / 45.5mM Na-Ace
pHi
7.5
7.45
7.4
7.35
7.3
7.25
7.2
7.15
7.1
7.05
0
20
40
60
80
100
120
140
Time (min)

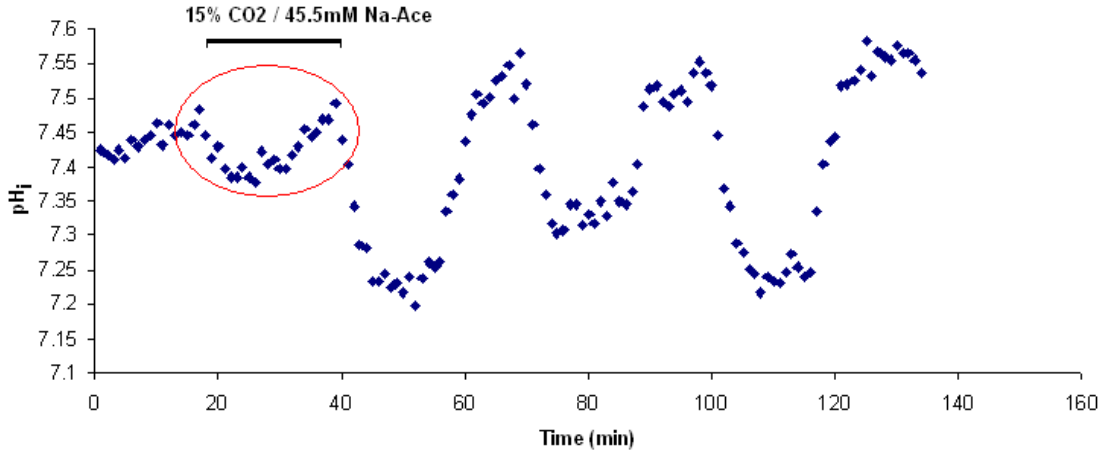
15% CO2 / 45.5mM Na-Ace
pHi
7.6
7.55
7.5
7.45
7.4
7.35
7.3
7.25
7.2
7.15
7.1
0
20
40
60
80
100
120
140
160
Time (min)

and does not require dissociation of the acid to free hydrogen. Thus, the initial acidification is not seen with the whole cell technique.

Effect of Acetic Acid in the NTS and LC

Acetic acid was the first acid used to test clamping with the weak-acid diffusion method within multiple neurons simultaneously in brainstem slices. A sample trace using an NTS neuron is shown in Figure 15A. The slice was first superfused with aCSF equilibrated with 5% CO_2 (pH_o ~7.45), then superfused with aCSF modified by adding 45.5mM (high) Na-acetate (Na-ace) (see Materials and Methods) and equilibrated with 5% CO_2 to load the cell with acid. Neurons were then exposed to the same solution equilibrated with 15% CO_2 (pH_o ~7.0) before returning to the previous 5% CO_2-equilibrated superfusate of the same Na-ace concentration. Cells were next superfused with an aCSF modified to contain 16.16mM (low) Na-acetate solution (see Materials and Methods) equilibrated with 15% CO_2, then superfused with the high Na-acetate solution equilibrated with 5% CO_2 once again. Lastly, neurons were exposed to a third bout of HA being superfused first with high Na-acetate equilibrated with 15% CO_2, then to 5% CO_2-equilibrated solution of the same concentration (45.5mM). Afterwards, the magnitudes of the three hypercapnia-induced acidifications were measured. To obtain the net change in pH_i for high extracellular acetate in hypercapnia, both of the acidifications were averaged before comparison against the acidification with low extracellular acetate. The same protocol was used for LC neurons, shown in the example LC trace in Figure 16A. Of the NTS cells tested (n = 56), a 33.1% blunting occurred with a pH change of 0.28 ± 0.008 with high acetate outside and 0.18 ± 0.009 with low acetate outside. The results were lower in LC neurons, with about 19.6% blunting and a pH change of 0.10 ± 0.008

FIGURE 15: Effect of hypercapnia and Na-acetate (Na-ace) on pH_i in NTS neurons using the weak acid diffusion technique with an inverted microscope. **A:** Individual trace of pH_i vs. time in a NTS neuron showing when hypercapnia (15% CO_2) and the concentrations of Na-ace, low (16.16mM) and high (45.5mM), were applied via the grey and black lines above the graph. Note that the two exposures to hypercapnia (15% CO_2) with high Na-ace concentrations each resulted in a substantial and similar acidification. The hypercapnic exposure using low Na-ace concentration also resulted in acidification, with the response blunted only slightly. **B:** Bar graph showing average hypercapnia-induced ΔpH_i in NTS neurons loaded with Na-acetate. The height of a bar indicates the mean ΔpH_i and the error bars represent 1 SEM. The number of neurons is indicated inside each bar and *** indicates the average values are very highly significantly different ($P<0.001$).

A.

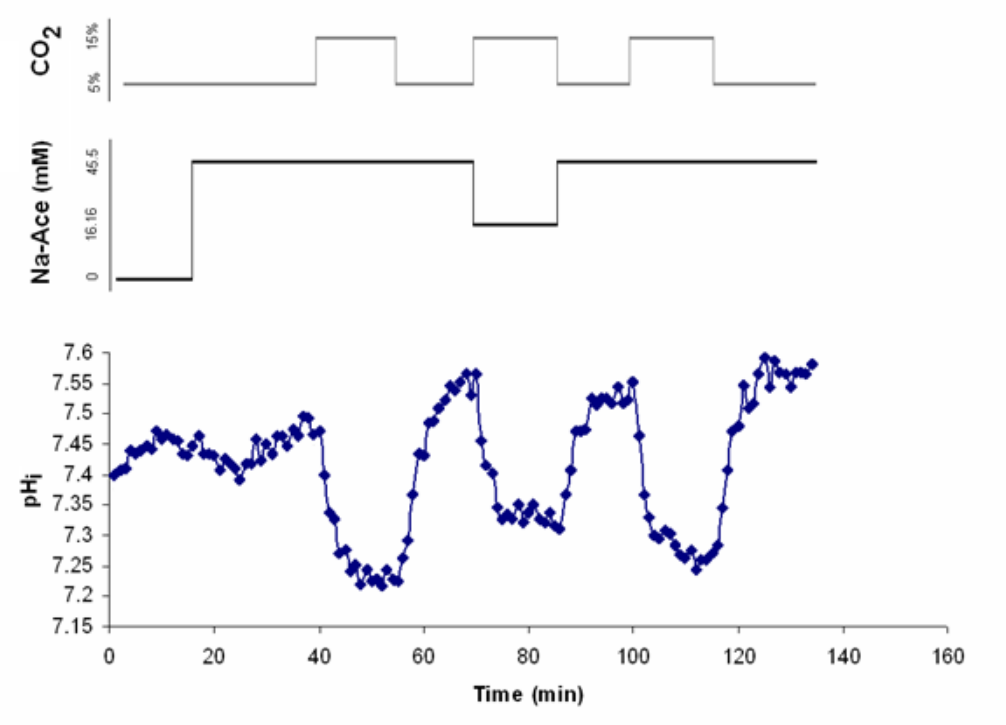
CO2
15%
5%
Na-Ace (mM)
45.5
16.16
0
pHi
7.6
7.55
7.5
7.45
7.4
7.35
7.3
7.25
7.2
7.15
0
20
40
60
80
100
120
140
160
Time (min)

B.

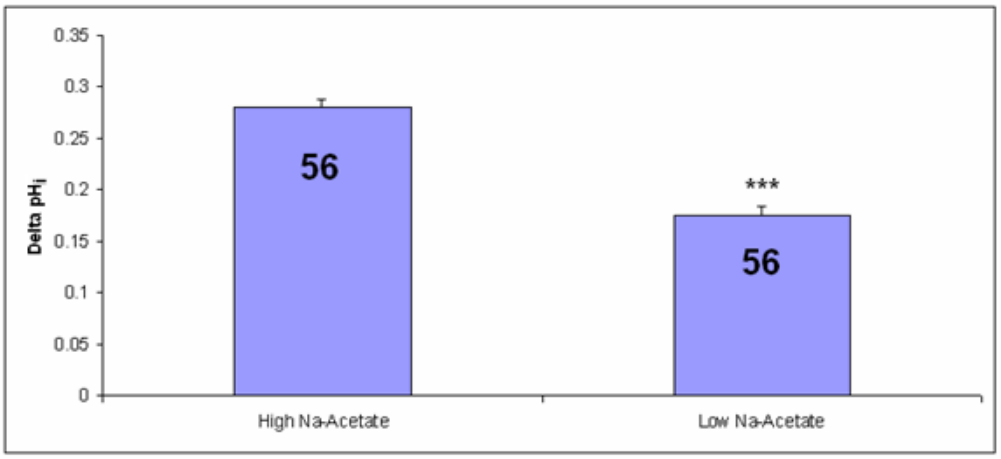
Delta pHi
0.35
0.3
0.25
0.2
0.15
0.1
0.05
0
56
***
56
High Na-Acetate
Low Na-Acetate

FIGURE 16: Effect of hypercapnia and Na-acetate (Na-ace) on pH_i in LC neurons using the weak-acid diffusion technique with an inverted microscope. **A:** Individual trace of pH_i vs. time in a LC neuron showing when hypercapnia (15% CO_2) and the concentrations of Na-ace, low (16.16mM) and high (45.5mM), were applied via the grey and black lines above. Note that the two exposures to hypercapnia (15% CO_2) with high Na-ace concentrations each resulted in a substantial and similar acidification. The hypercapnic exposure using low Na-ace concentration also resulted in acidification, with the response blunted only slightly. **B:** Bar graph showing average hypercapnia-induced ΔpH_i in LC neurons loaded with Na-acetate. The height of a bar indicates the mean ΔpH_i and the error bars represent 1 SEM. The number of neurons is indicated inside each bar and * indicates the average values are significantly different ($P<0.05$).

A.

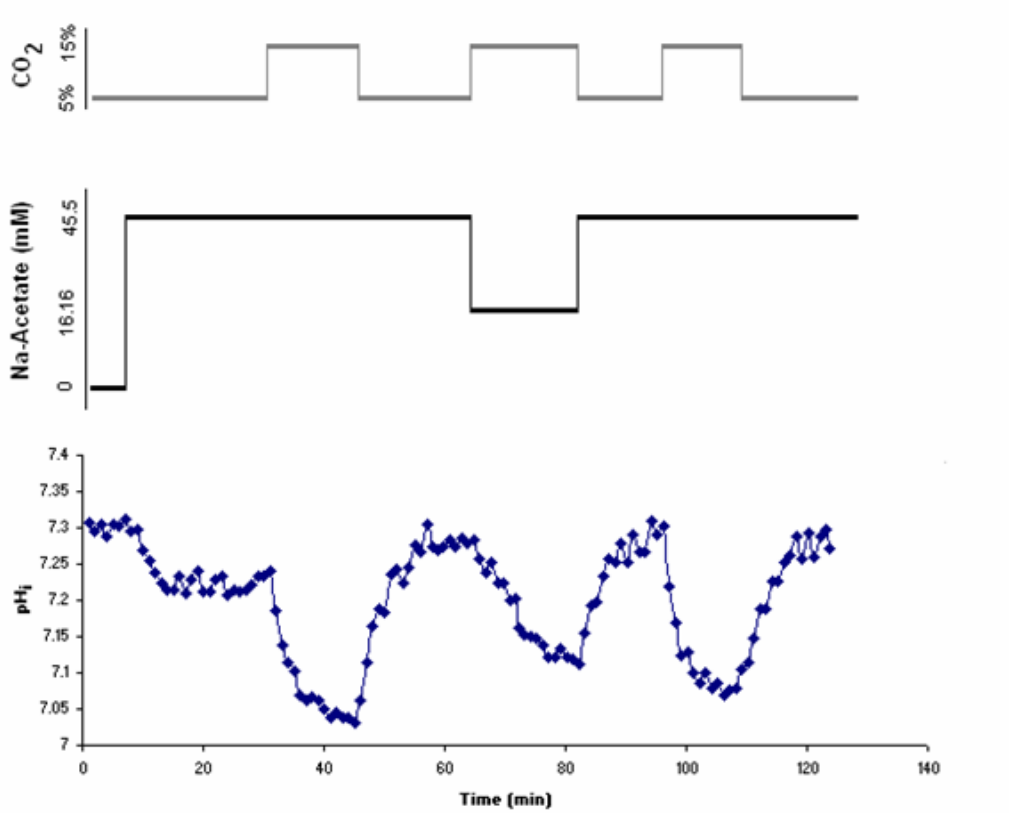
CO_2
15%
5%
Na-Acetate (mM)
45.5
16.16
0
pH_i
7.4
7.35
7.3
7.25
7.2
7.15
7.1
7.05
7
0
20
40
60
80
100
120
140
Time (min)

B.

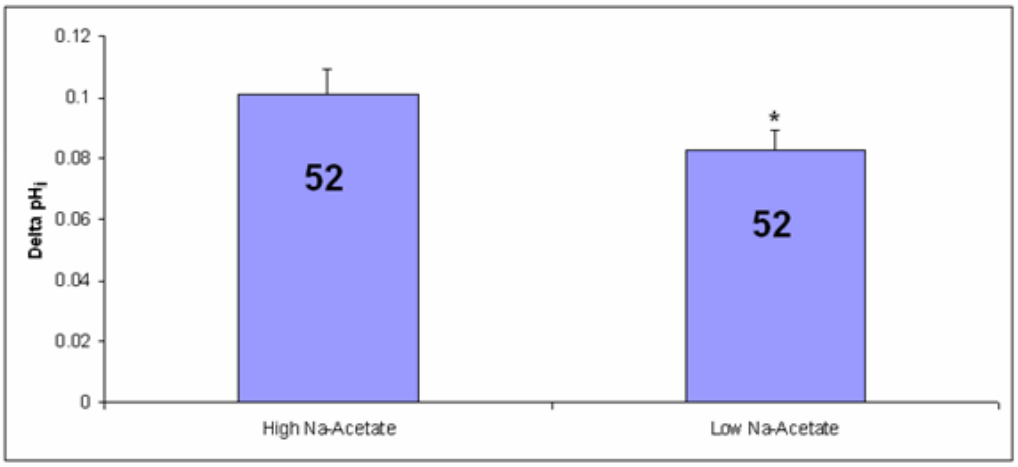
Delta pH_i
0.12
0.1
0.08
0.06
0.04
0.02
0
52
52
*
High Na-Acetate
Low Na-Acetate

and 0.08 ± 0.007 for high and low concentrations outside, respectively (n = 52). These averages are shown as bar graphs in Figure 15B and 16B for NTS and LC neurons, respectively.

Of the NTS traces, however, 7 cells from the same slice from one rat exhibited relatively superb clamping, with an average blunting of ~ 81.5%. An example trace of a cell from this slice is shown in Figure 17, implying variability in the effectiveness of pH_i clamping. Upon calculating the NTS cells without the 7 cells (n = 49), the percent blunting in NTS neurons drops to ~16.9%, with a pH change of 0.24 ± 0.002 and ~0.20 ± 0.003 in high and low outside concentrations, respectively.

Differences in the net change of pH values between low and high acetate concentrations outside the cell were very highly significant ($P<0.001$) in the NTS region, both if one includes the aforementioned 7 cells and if one does not. For the LC region, the value was significant ($P<0.05$), indicating that Na-acetate produced similar net pH_i changes for both concentrations in LC and in NTS. Differences comparing the LC and NTS values of outside high acetate and outside low acetate were both found to be very highly significant, with a $P<0.001$.

The degree of blunting (20-24%) using the loading of acetic acid, except for one NTS slice (82%), was very disappointing. We hypothesized that the degree of blunting may be related to how much acid was initially loaded into the neurons. Based on this assumption, we reasoned that the degree of the initial acidification induced by exposure to acetic acid should be positively correlated with the degree of blunting, the former indicating greater weak acid loading which would give rise to a higher blunting. Such an analysis is shown in Figure 18. In fact, the relationship between the initial

FIGURE 17: Unique trace of pH_i vs. time in a NTS neuron showing the effect of hypercapnia and Na-acetate (Na-ace) using the weak-acid diffusion technique with an inverted microscope. Bouts of hypercapnia (15% CO_2) and the concentrations of Na-ace, low (16.16mM) and high (45.5mM), are shown via the grey and black lines above the graph. Note that the two exposures to hypercapnia (15% CO_2) with high Na-ace concentrations each resulted in a substantial and similar acidification. In contrast, in the presence of low Na-ace concentration, hypercapnia-induced acidification was considerably smaller. This example suggests blunting variability compared to the otherwise low pH_i blunting average of Na-acetate in neonatal NTS neurons.

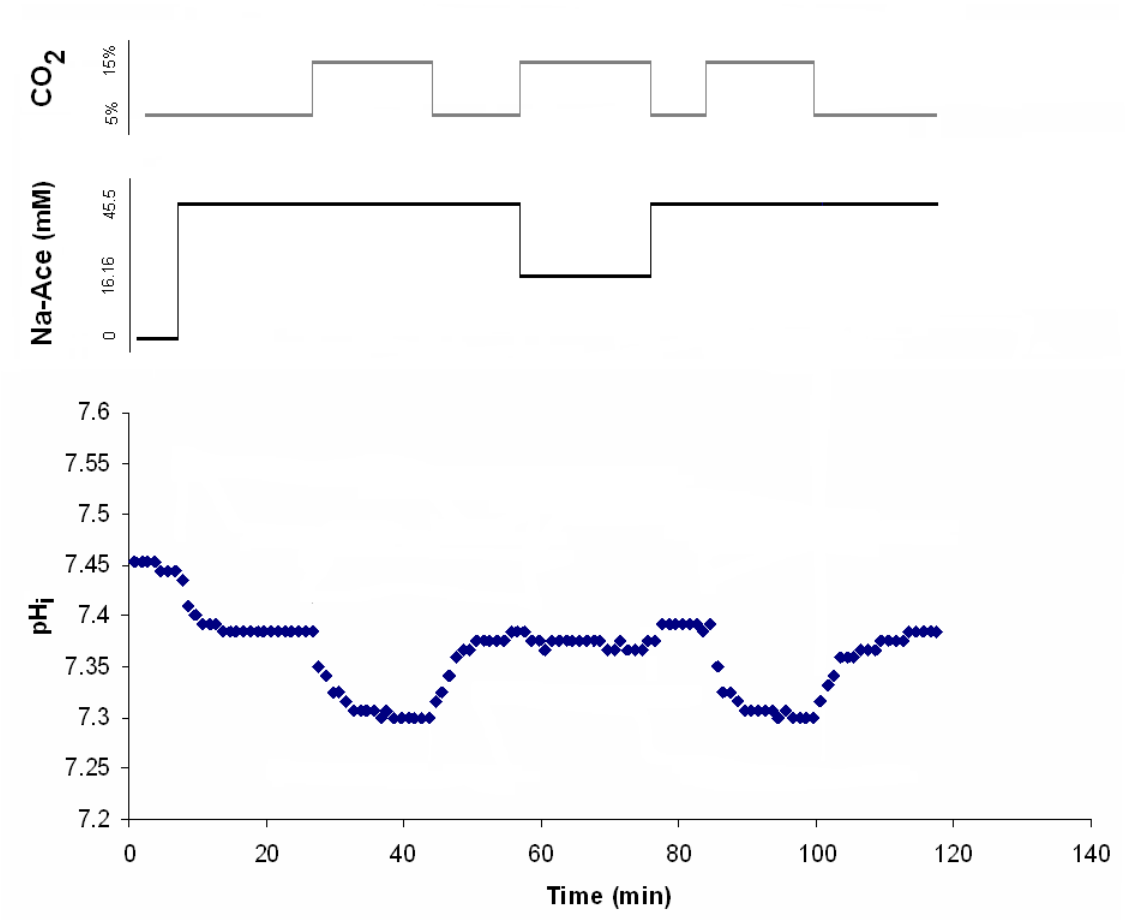
CO_2
15%
5%
Na-Ace (mM)
45.5
16.16
0
pH_i
7.6
7.55
7.5
7.45
7.4
7.35
7.3
7.25
7.2
0
20
40
60
80
100
120
140
Time (min)

acidification induced by acetic acid exposure and the degree of blunting is inverse, not direct, indicating that our initial assumption that the degree of blunting is due to poor acid loading is not valid.

Effect of TMA in the NTS and LC

Although the use of Na-acetate was able to blunt pH_i changes induced by acid exposure, it did so only poorly. In an attempt to blunt multiple cells simultaneously in brainstem slices using a different approach, we added a weak base, trimethyl amine (TMA), along with the exposure to hypercapnia to create a counterbalancing influx of base (TMA) along with the hypercapnia-induced acidification in an attempt to clamp pH_i during hypercapnia. The slice was first superfused with aCSF equilibrated with 5% CO_2 (pH_o ~7.45), then superfused with aCSF equilibrated with 15% CO_2 (pH_o ~7.00), i.e. one bout of hypercapnia. The slice was then superfused with a 20mM TMA solution (see Materials and Methods) equilibrated with 15% CO_2 (the base and acid together) before being returned to 5% CO_2-equilibrated aCSF. The magnitudes of the acidifications were then measured and compared. Two traces using TMA are shown in Figures 18A and 19A, the first using an NTS neuron and the second an LC neuron. The averages of the NTS and LC regions were similar to each other, but the overall effect was that of an increased, not decreased, acidification. Figures 19B and 20B show these averages in bar graph form. In the NTS (n = 40), there was no blunting (a calculated value of -18.1%) (pH changes = 0.22 ± 0.004 with and 0.19 ± 0.003 without TMA) and in the LC (n = 28) there was also no blunting (a calculated value of -27.8%) (pH changes = 0.17 ± 0.036 with and ~0.13 ± 0.005 without TMA). These differences from the NTS and LC regions were very highly significant ($P<0.001$ for both regions).

FIGURE 18. Relationship of percent blunting and initial pH_i change using Na-acetate. **A:** Plot of percent pH_i blunting vs. initial ΔpH_i in NTS neurons from the Na-acetate experiments. A linear regression line is applied, resulting in the equation % blunting = -248.92(initial ΔpH_i) + 50.423 with an R^2 value of 0.2585. Note that the slope of the correlation is negative, suggesting that the final blunting response decreases with an increasing initial weak acid load. This plot includes the 7 well-blunted "outlier" cells reported in the Results section, circled in red. **B:** Plot of percent pH_i blunting vs. initial ΔpH_i in NTS neurons from the Na-acetate experiments with the 7 well-blunted "outlier" cells removed. A linear regression line is applied, resulting in the equation % blunting = -82.212(initial ΔpH_i) + 25.559 with an R^2 value of 0.2188. Note that despite removal of the outliers, the negative slope remains and is still suggestive of an inversely proportional relationship between final % blunting and initial pH_i change. **C:** Plot of percent pH_i blunting vs. initial ΔpH_i in LC neurons from the Na-acetate experiments. A linear regression line is applied, resulting in the equation y = -257.2x + 32.109with an R^2 value of 0.5748. Note that the slope here is also negative.

A.

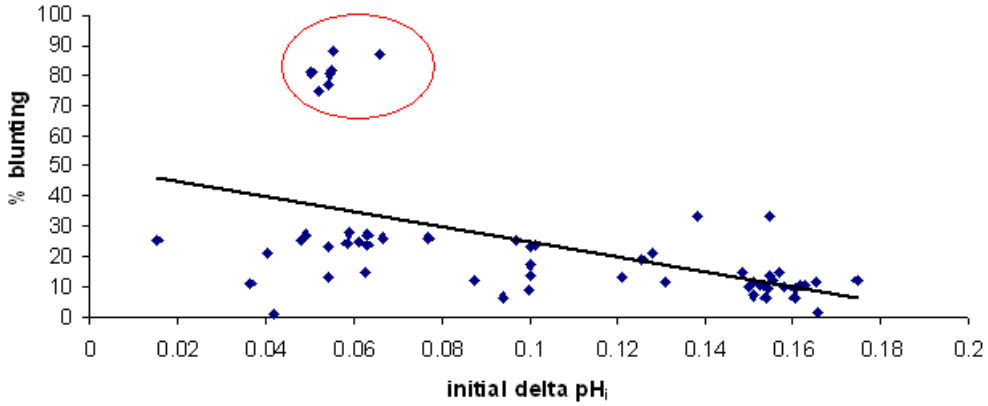
% blunting
initial delta pH$_i$

B.

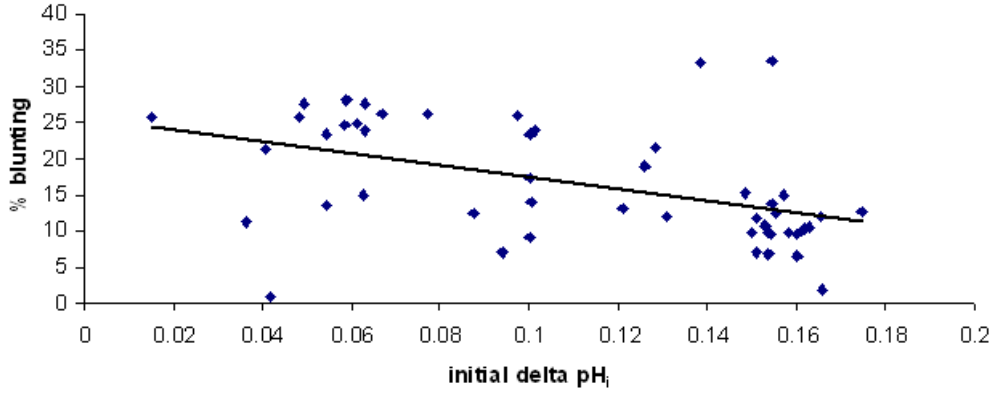
% blunting
initial delta pH$_i$

C.

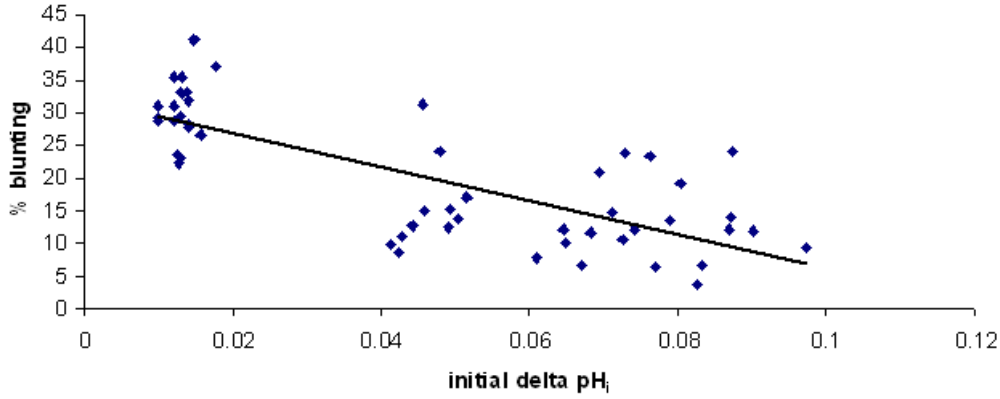
% blunting
initial delta pH$_i$

FIGURE 19: Effect of hypercapnia and trimethyl amine (TMA) on pH_i in NTS neurons using an inverted microscope. **A:** Individual trace of pH_i vs. time in a NTS neuron showing when hypercapnia (15% CO_2) and TMA (20mM) were applied via the grey and black lines above the graph. Note that the exposure to hypercapnia (15% CO_2) with TMA resulted in a substantial acidification slightly greater than the hypercapnia-induced acidification in aCSF. **B:** Bar graph showing average hypercapnia-induced ΔpH_i in NTS neurons using TMA. The height of a bar indicates the mean ΔpH_i and the error bars represent 1 SEM. The number of neurons is indicated inside each bar and *** indicates the average values are very highly significantly different ($P<0.001$).

A.

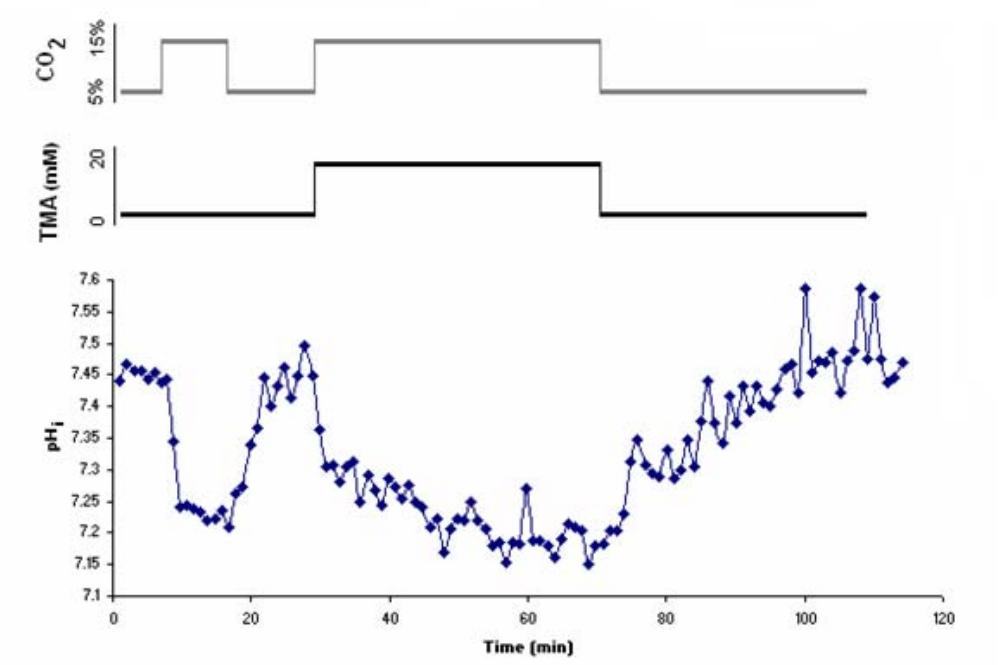
CO_2
15%
5%
TMA (mM)
20
0
pH_i
7.6
7.55
7.5
7.45
7.4
7.35
7.3
7.25
7.2
7.15
7.1
0
20
40
60
80
100
120
Time (min)

B.

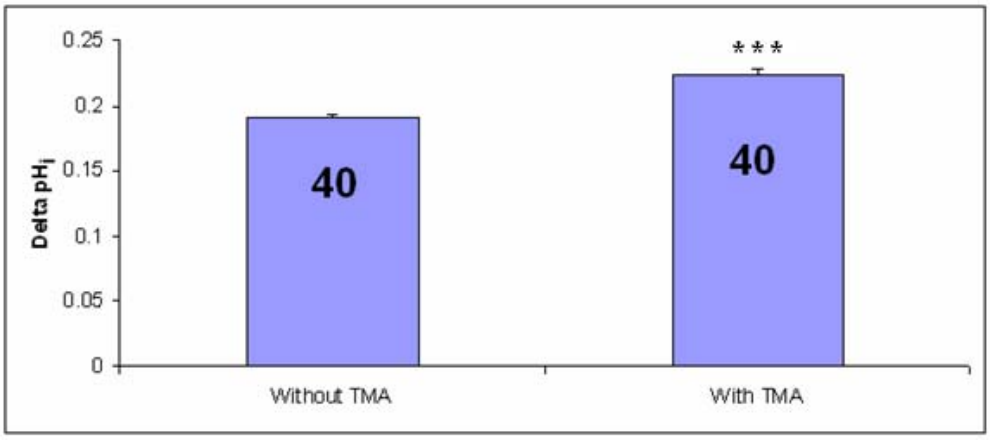
Delta pH_i
0.25
0.2
0.15
0.1
0.05
0
* * *
40
40
Without TMA
With TMA

FIGURE 20: Effect of hypercapnia and trimethyl amine (TMA) on pH_i in LC neurons using an inverted microscope. **A:** Individual trace of pH_i vs. time in a LC neuron showing when hypercapnia (15% CO_2) and TMA (20mM) were applied via the grey and black lines above the graph. Note that, like in the NTS neuron with TMA, the exposure to hypercapnia (15% CO_2) with TMA resulted in a substantial acidification greater than the hypercapnia-induced acidification in aCSF. **B:** Bar graph showing average hypercapnia-induced ΔpH_i in NTS neurons using TMA. The height of a bar indicates the mean ΔpH_i and the error bars represent 1 SEM. The number of neurons is indicated inside each bar and *** indicates the average values are very highly significantly different ($P<0.001$).

A.

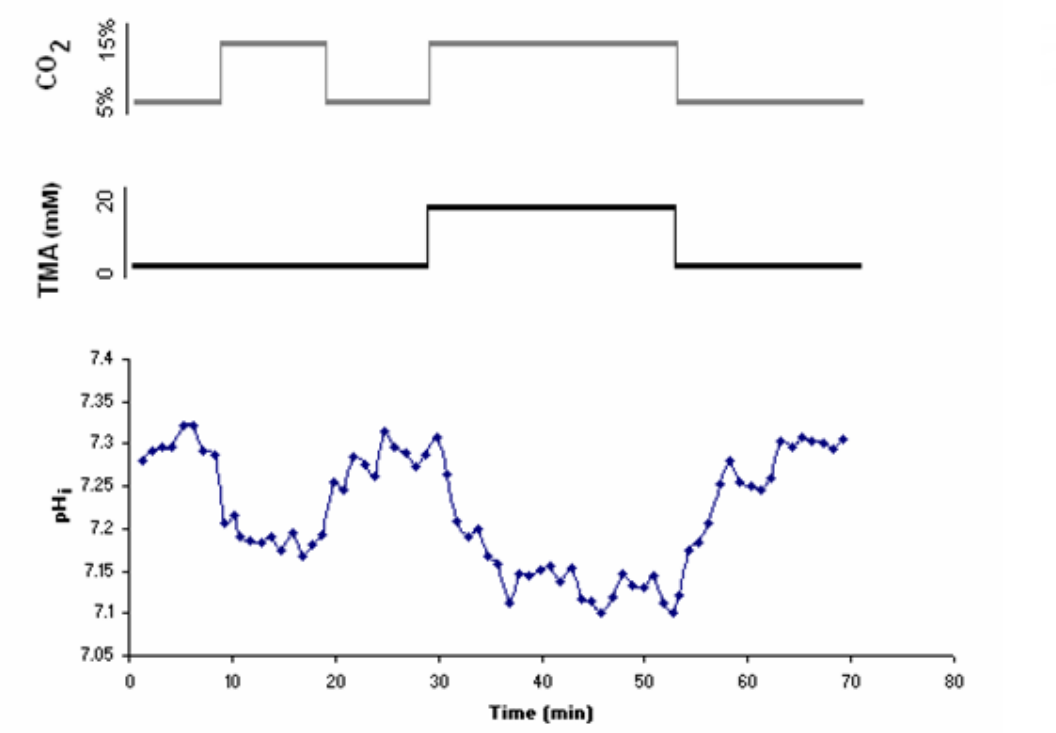
CO_2
15%
5%
TMA (mM)
20
0
pH_i
7.4
7.35
7.3
7.25
7.2
7.15
7.1
7.05
0
10
20
30
40
50
60
70
80
Time (min)

B.

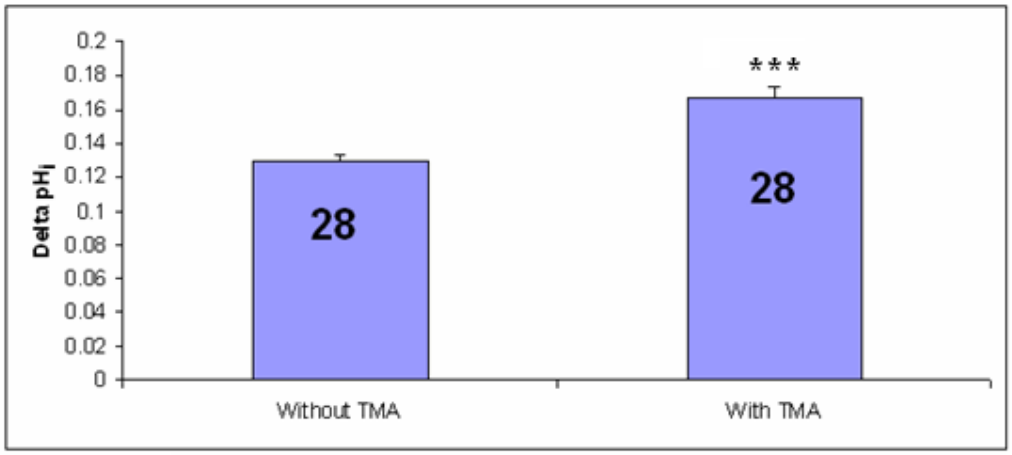
Delta pH_i
0.2
0.18
0.16
0.14
0.12
0.1
0.08
0.06
0.04
0.02
0
***
28
28
Without TMA
With TMA

Effect of Caproic Acid in the NTS and LC

Given that the diffusion of weak base with HA-induced acidification to blunt pH_i was unsuccessful, attention was turned back to the possibility that difficulties with the initial loading of weak acid across the cell membrane prevented more effective blunting. If weak acid does not substantially load into the cell in the first place, there can be no efflux of H^+ to blunt the acidification upon exposure to hypercapnia. In order to address the concern of limited acid diffusion, acetic acid was replaced by another weak acid, caproic acid. Caproic acid (or hexanoic acid) is a six-carbon-chain weak acid that has four more carbon atoms than acetic acid, thus it should more readily diffuse across the membrane due to its increased lipophilic nature.

Caproic acid was therefore the second acid used to test clamping with the weak-acid diffusion method within multiple neurons simultaneously in brainstem slices. A sample trace using Na-caproate (Na-cap) in an NTS neuron is shown in Fig. 21A. The slice was first superfused with aCSF equilibrated with 5% CO_2 (pH_o ~7.45), then superfused with aCSF modified by adding 45.5mM (high) Na-caproate (see Materials and Methods) and equilibrated with 5% CO_2 to load the cell with acid. Cells were next superfused with aCSF modified by adding16.16mM (low) Na-caproate (see Materials and Methods) and equilibrated with 15% CO_2, then superfused with the high Na-caproate solution equilibrated with 5% CO_2. Neurons were then exposed to the high (45.5mM) solution equilibrated with 15% CO_2 (pH_o ~7.0) before returning to the previous 5% CO_2-equilibrated superfusate of the same Na-cap concentration. Afterwards, the magnitudes of the two hypercapnia-induced acidifications were measured. The same protocol was used for LC neurons, shown in Fig. 22A.

FIGURE 21: Effect of hypercapnia and Na-caproate (Na-cap) on pH_i in NTS neurons using the weak-acid diffusion technique using an inverted microscope. **A:** Individual trace of pH_i vs. time in a NTS neuron showing when hypercapnia (15% CO_2) and the concentrations of Na-cap, low (16.16mM) and high (45.5mM), were applied via the grey and black lines above the graph. An initial acidification is seen due to the loading of Na-cap into the cell. Note that the exposure to hypercapnia (15% CO_2) with high Na-cap concentrations resulted in a substantial acidification. In comparison, the hypercapnic exposure using low Na-cap concentration also acidified but with a blunting response of about 50%. **B:** Bar graph showing average hypercapnia-induced ΔpH_i in NTS neurons loaded with Na-caproate. The height of a bar indicates the mean ΔpH_i and the error bars represent 1 SEM. The number of neurons is indicated inside each bar and *** indicates the average values are very highly significantly different ($P<0.001$).

A.

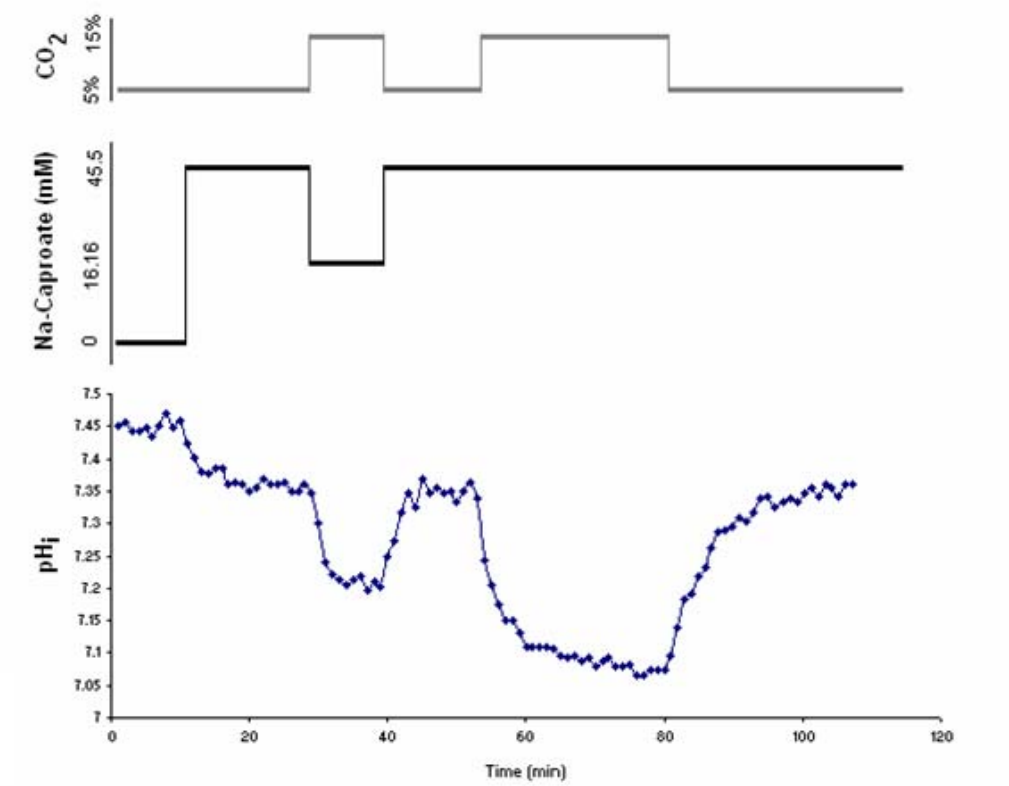
CO_2
5%
15%
Na-Caproate (mM)
0
16.16
45.5
pH_i
7.5
7.45
7.4
7.35
7.3
7.25
7.2
7.15
7.1
7.05
7
0
20
40
60
80
100
120
Time (min)

B.

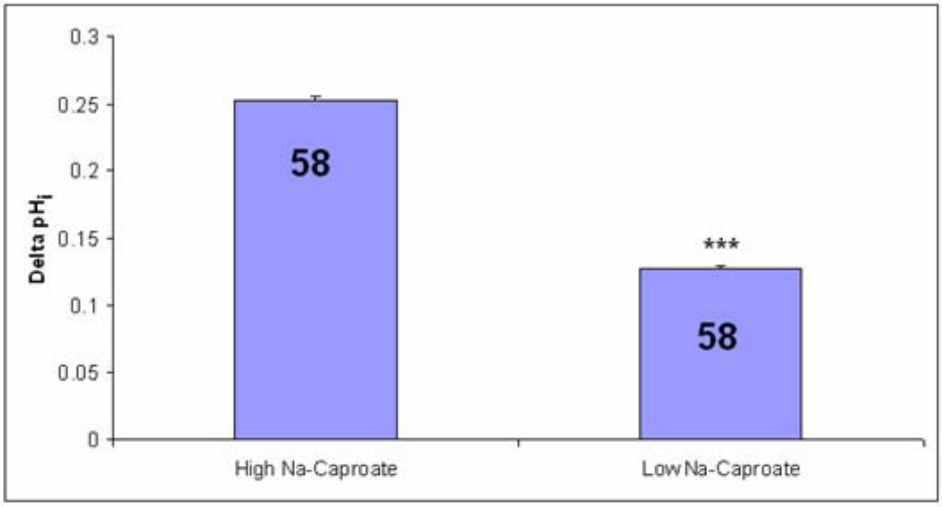
Delta pH_i
0.3
0.25
0.2
0.15
0.1
0.05
0
58
***
58
High Na-Caproate
Low Na-Caproate

The averages of these experiments are shown in Fig. 21B and 22B for the NTS and LC regions, respectively. When using Na-caproate, percent blunting increased in both regions. In the NTS region, a 50.7% pH_i blunting occurred (n = 58), and in the LC, a 45.8% blunting (n = 47), a little more than twice the blunting effectiveness of Na-acetate in both regions. The pH changes were 0.25 ± 0.004 and 0.13 ± 0.002 for high and low concentrations of Na-caproate in NTS, and ~0.21 ± 0.003 and ~0.11 ± 0.002 for high and low Na-caproate in LC. These differences were very highly significant, with a $P<0.001$ for both regions. Overall, these data suggest that blunting is improved with more permeable weak acids.

We once again analyzed the relationship between the degree blunting as a function of the initial acidification induced upon exposure to caproic acid as we did for acetic acid (Figure 23). In this case there was at most a small positive relationship between these two parameters and in effect there was no significant correlation between the two. Thus, once again, the initial degree of acidification induced by exposure to caproic acid does not seem to be a good predictor of the degree of blunting.

Upright vs. Inverted Microscopes

While blunting was enhanced with increased membrane permeability, it still did not clamp pH_i completely. We then considered perfusion limitations that might also prevent both the loading of weak acid into the cell as well as the overall acid exposure up to the cell itself. One of these limitations might be caused by the use of an inverted microscope that views cells on the bottom of a slice. These cells are probably superfused more poorly since they are covered by the layers of tissue above and pressed against the Plexiglas floor of the superfusion chamber on which they sit. To address this, the

FIGURE 22: Effect of hypercapnia and Na-caproate (Na-cap) on pH_i in LC neurons using the weak-acid diffusion technique using an inverted microscope. **A:** Individual trace of pH_i vs. time in a LC neuron showing when hypercapnia (15% CO_2) and the concentrations of Na-cap, low (16.16mM) and high (45.5mM), were applied via the grey and black lines above the graph. Note that the exposure to hypercapnia (15% CO_2) with high Na-cap concentrations resulted in a substantial acidification. In comparison, the hypercapnic exposure using low Na-cap concentration also acidified but with a blunting response of about 50%, similar to pH_i blunting with Na-cap in the NTS neurons. **B:** Bar graph showing average hypercapnia-induced ΔpH_i in NTS neurons loaded with Na-caproate. The height of a bar indicates the mean ΔpH_i and the error bars represent 1 SEM. The number of neurons is indicated inside each bar and *** indicates the average values are very highly significantly different ($P<0.001$).

A.

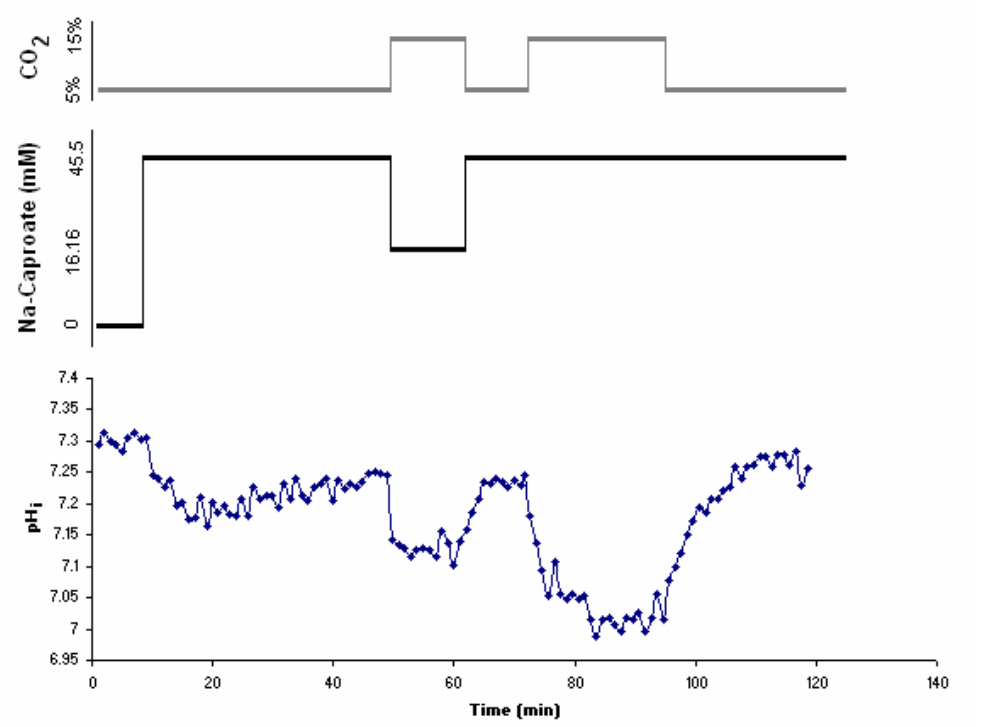
CO_2
15%
5%
Na-Caproate (mM)
45.5
16.16
0
pH_i
7.4
7.35
7.3
7.25
7.2
7.15
7.1
7.05
7
6.95
0
20
40
60
80
100
120
140
Time (min)

B.

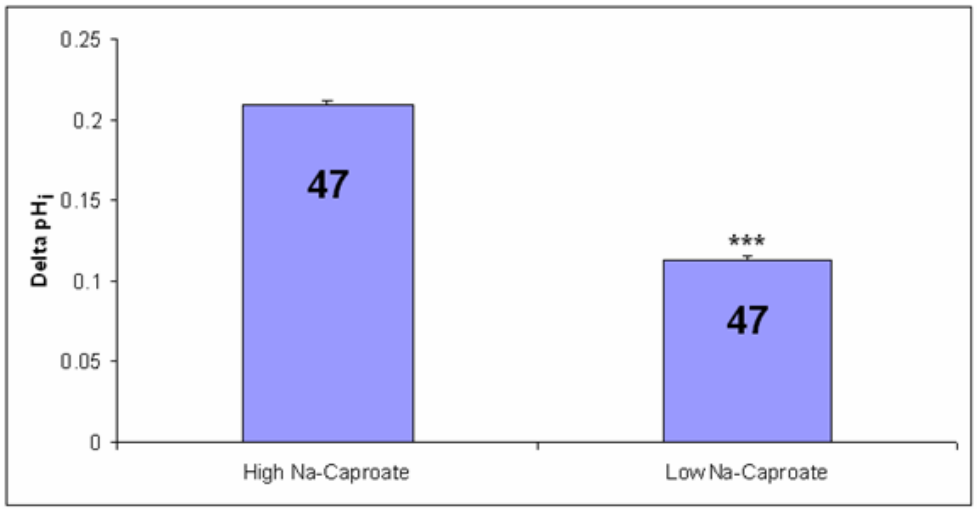
Delta pH_i
0.25
0.2
0.15
0.1
0.05
0
47
***
47
High Na-Caproate
Low Na-Caproate

FIGURE 23. Relationship of percent blunting and initial pH_i change using Na-caproate. **A:** Plot of percent pH_i blunting vs. initial ΔpH_i in NTS neurons from the Na-caproate experiments. A linear regression line is applied, resulting in equation % blunting = 70.276(initial ΔpH_i) + 41.497 with an R^2 value of 0.2076. Note that the slope of the correlation is slightly positive, suggesting that the final blunting response increases with increasing initial weak acid load. **B:** Plot of percent pH_i blunting vs. initial ΔpH_i in LC neurons from the Na-caproate experiments. A linear regression line is applied, resulting in the equation % blunting = -45.994(initial ΔpH_i) + 50.306 with an R^2 value of 0.0269. Note that unlike the NTS cells using the same weak acid, the slope of the correlation is negative and suggestive of an inversely proportional relationship between final % blunting and initial pH_i change.

A.

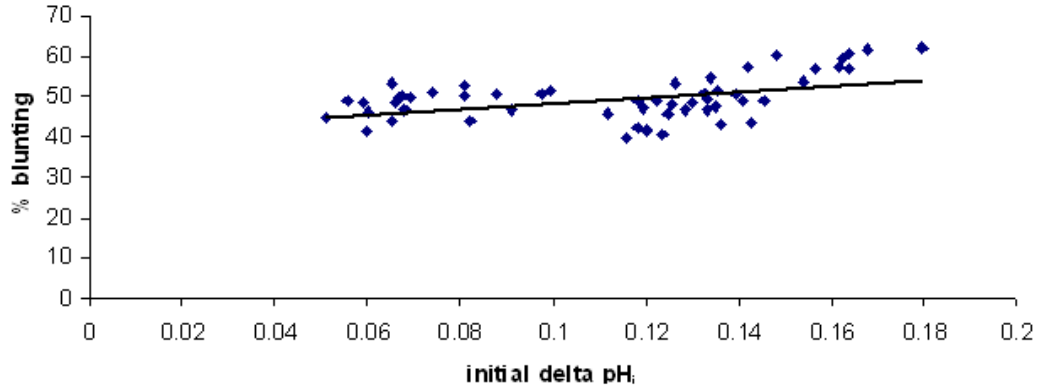
% blunting
70
60
50
40
30
20
10
0
0
0.02
0.04
0.06
0.08
0.1
0.12
0.14
0.16
0.18
0.2
initial delta pH$_i$

B.

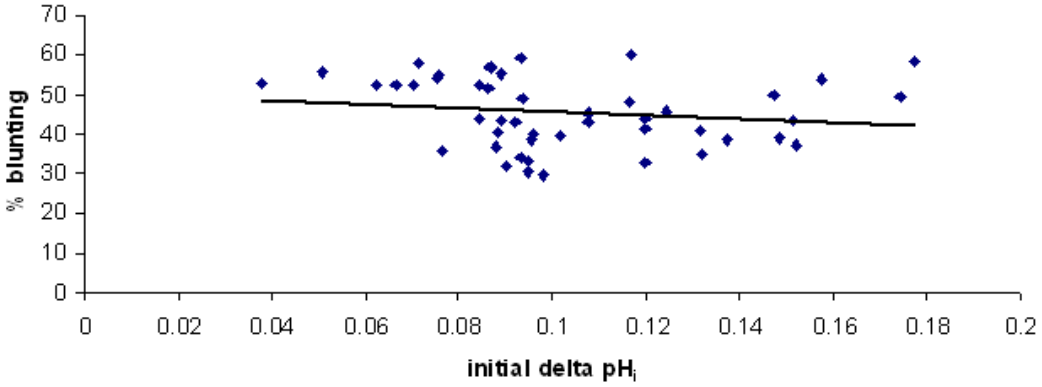
% blunting
70
60
50
40
30
20
10
0
0
0.02
0.04
0.06
0.08
0.1
0.12
0.14
0.16
0.18
0.2
initial delta pH$_i$

experimental setup was switched to an upright microscope with the same protocol as that used previously for the Na-acetate experiments, with the same concentrations and order of superfusate, and in multiple cells simultaneously in brainstem slices. Given that the upright objective views the cells on the uppermost layers of the brain slice instead of the bottom, and that the top layer cells are directly exposed to the flow of solution, we reasoned cells studied with the upright microscope should be better superfused and thus should show better weak acid loading and therefore better blunting (Figure 24).

Using the upright microscope, the Na-acetate experiments were repeated and the following blunting percentages produced: 45.8% blunting in the NTS (pH change = 0.18 ± with 0.009 high and 0.10 ± 0.013 with low,) and 52.6% blunting in the LC (pH change = ~0.13 ± 0.005 with high and 0.06 ± 0.009 with low Na-acetate). Example traces from individual NTS and LC neurons are shown in Fig. 25A and 26A, respectively, and the averages from the NTS and LC regions are shown in bar graphs in Fig. 25B and 26B. These differences were statistically very highly significant with a $P<0.001$. In comparison with the Na-acetate experiments using an inverted microscope, blunting percentages at least doubled in both regions when using an upright microscope. Fig. 27, for example, shows an overlay of Fig. 15A and 25A on the same graph. We see that hypercapnia induces a reversible acidification of about 0.2 pH unit using an inverted microscope (the blue line). In contrast, the use of an upright microscope reduced the acidification induced by hypercapnia, inducing a reversible acidification of about 0.1 pH unit (the pink line). These data overall suggest that pH_i blunting is improved with better superfusion, i.e. the use of an upright microscope.

FIGURE 24. Drawing of inverted and upright objectives on a single stage. Perfusion limitations were speculated with the use of an inverted microscope, where only cells at the bottom of the slice would bevisualized. Physically, these neurons are surrounded on all sides by the Plexiglas floor and the tissue above. An upright scope, however, would not have the issue of viewing these because its objective instead looks at cells directly exposed to the flow of solution. These "upper" cells were hypothesized and shown to be better superfused because of their location in the slice and bath.

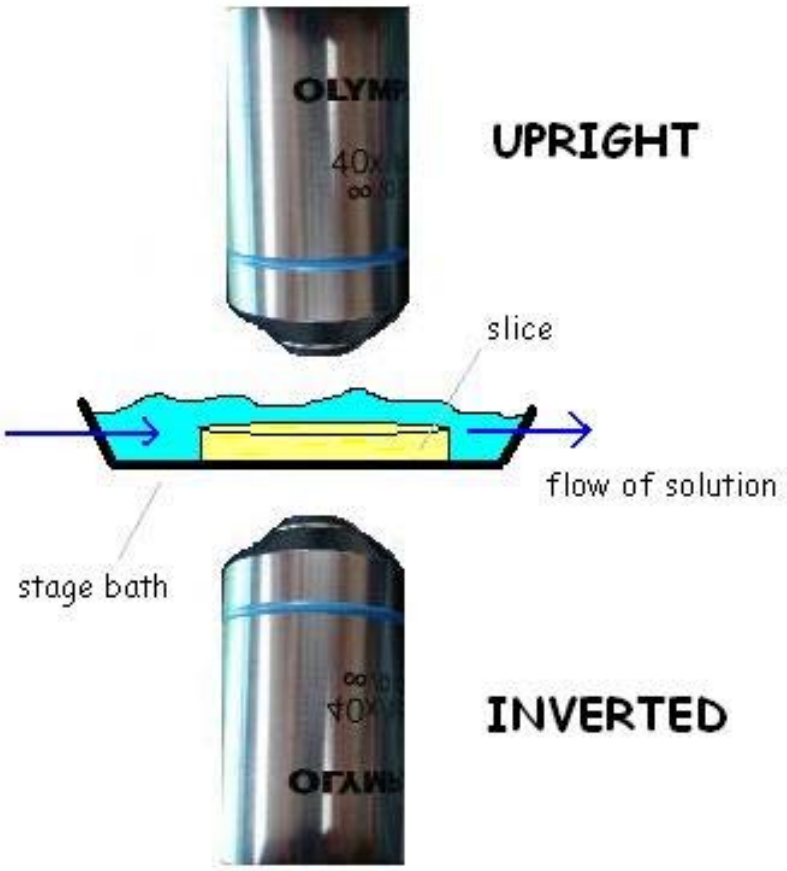
UPRIGHT
slice
flow of solution
stage bath
INVERTED

FIGURE 25: Effect of hypercapnia and Na-acetate (Na-ace) on pH_i in NTS neurons with the weak-acid diffusion technique using an upright microscope. **A:** Individual trace of pH_i vs. time in a NTS neuron showing when hypercapnia (15% CO_2) and the concentrations of Na-ace, low (16.16mM) and high (45.5mM), were applied via the grey and black lines above the graph. Note that the two exposures to hypercapnia (15% CO_2) with high Na-ace concentrations resulted in substantial and similar acidifications. In comparison, the hypercapnic exposure using low Na-ace concentration also acidified but with a blunting response of about 46%. **B:** Bar graph showing average hypercapnia-induced ΔpH_i in Na-acetate loaded NTS neurons visualized with an upright scope. The height of a bar indicates the mean ΔpH_i and the error bars represent 1 SEM. The number of neurons is indicated inside each bar and *** indicates the average values are very highly significantly different ($P<0.001$).

A.

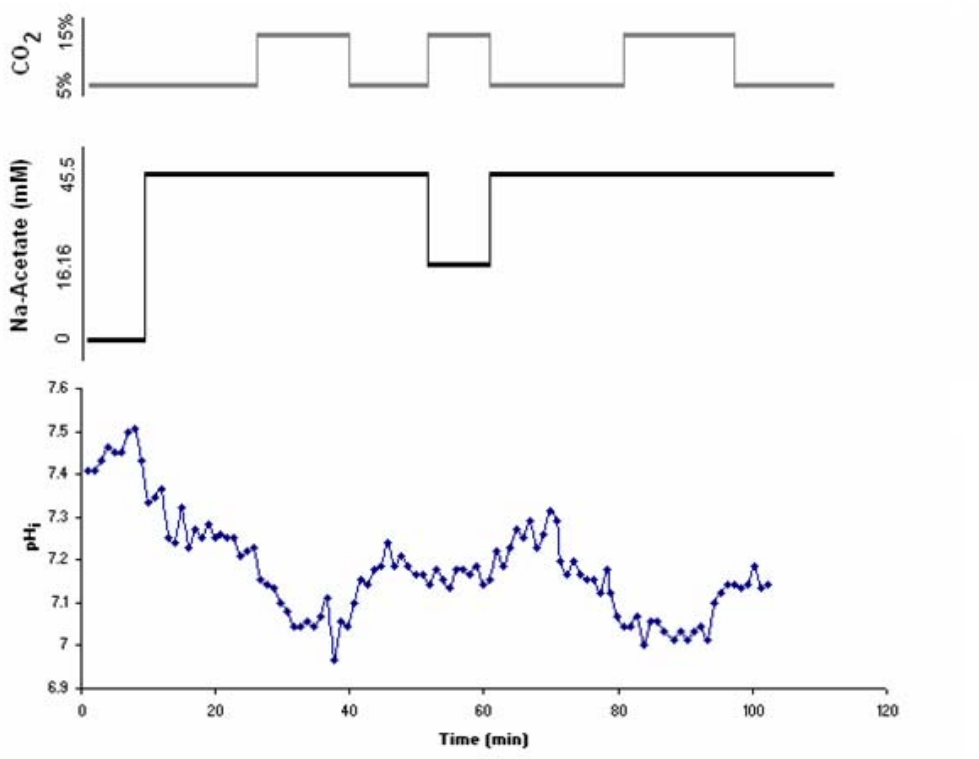
CO2
5%
15%
Na-Acetate (mM)
0
16.16
45.5
pHi
7.6
7.5
7.4
7.3
7.2
7.1
7
6.9
0
20
40
60
80
100
120
Time (min)

B.

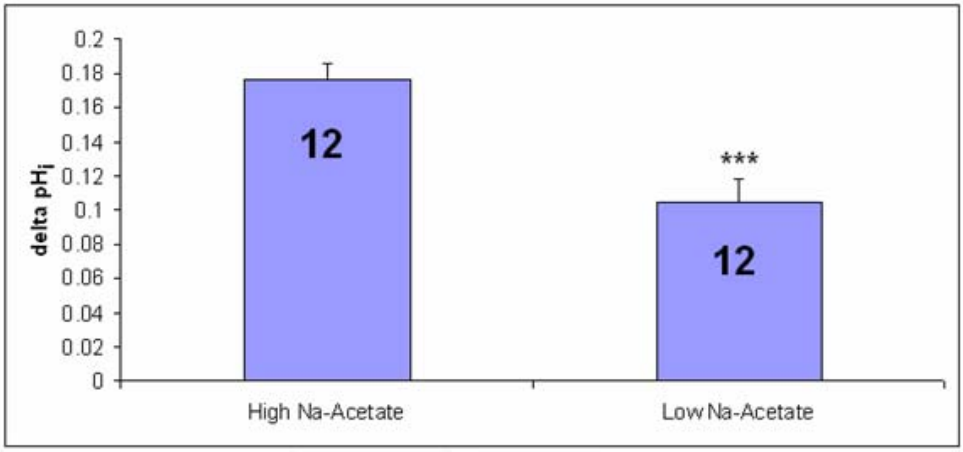
delta pHi
0.2
0.18
0.16
0.14
0.12
0.1
0.08
0.06
0.04
0.02
0
12
***
12
High Na-Acetate
Low Na-Acetate

FIGURE 26: Effect of hypercapnia and Na-acetate (Na-ace) on pH_i in LC neurons with the weak-acid diffusion technique using an upright microscope. **A:** Individual trace of pH_i vs. time in a LC neuron showing when hypercapnia (15% CO_2) and the concentrations of Na-ace, low (16.16mM) and high (45.5mM), were applied via the grey and black lines above the graph. Note that the two exposures to hypercapnia (15% CO_2) with high Na-ace concentrations resulted in substantial and similar acidifications. In comparison, the hypercapnic exposure using low Na-ace concentration also acidified but with a blunting response of about 53%, similar to the NTS trace with the upright setup. **B:** Bar graph showing average hypercapnia-induced ΔpH_i in Na-acetate loaded LC neurons visualized with an upright microscope. The height of a bar indicates the mean ΔpH_i and the error bars represent 1 SEM. The number of neurons is indicated inside each bar and *** indicates the average values are very highly significantly different ($P<0.001$).

A.

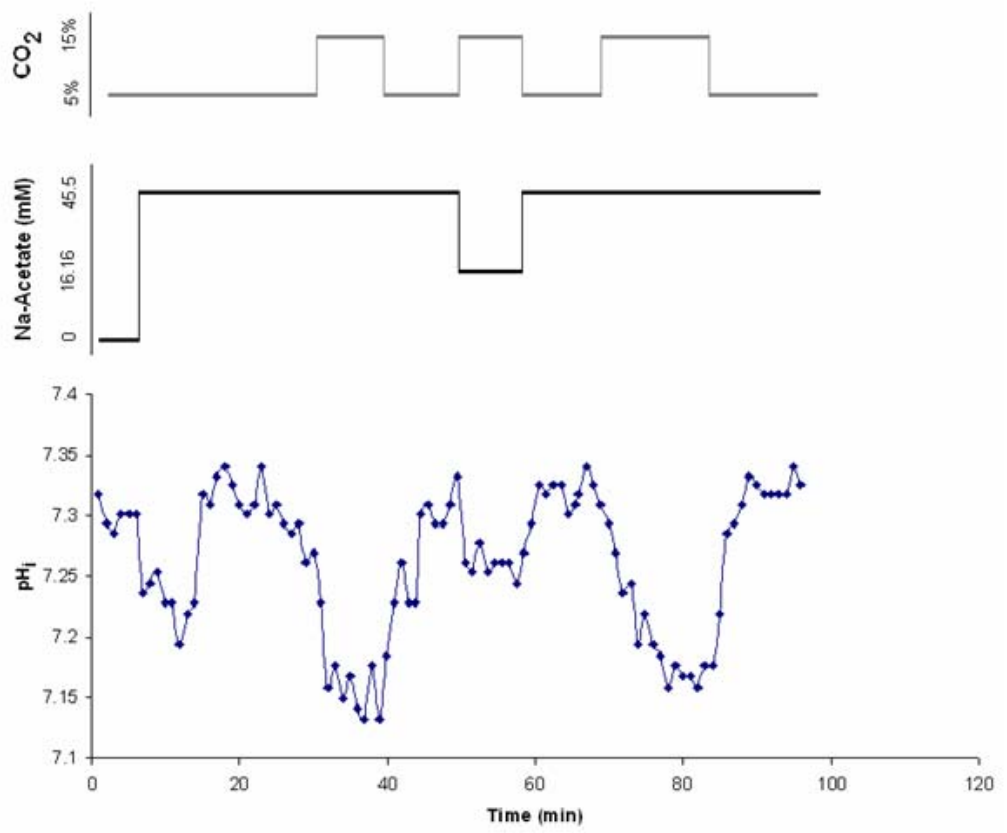
CO_2
15%
5%
Na-Acetate (mM)
45.5
16.16
0
pH_i
7.4
7.35
7.3
7.25
7.2
7.15
7.1
0
20
40
60
80
100
120
Time (min)

B.

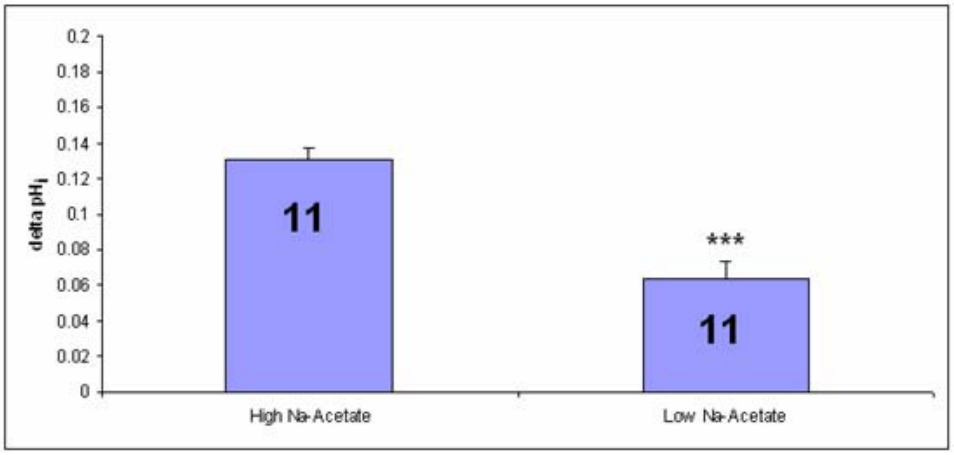
delta pH_i
0.2
0.18
0.16
0.14
0.12
0.1
0.08
0.06
0.04
0.02
0
11
***
11
High Na-Acetate
Low Na-Acetate

FIGURE 27. Trace overlay of figures 15A and 25A (Na-acetate runs in NTS neurons) comparing the use of an upright vs. inverted microscope on the same graph. Timing of the superfusates differs between the two cells because all runs were completed based on plateau responses to each change of solution and CO_2. Instead, compare the hypercapnia-induced acidifications where [Na-acetate] was lowered in contrast to the hypercapnia-induced acidifications in the presence of [high] Na-acetate, shown in the second pH_i drop of the total three (see previous figures for solution and gas markings).

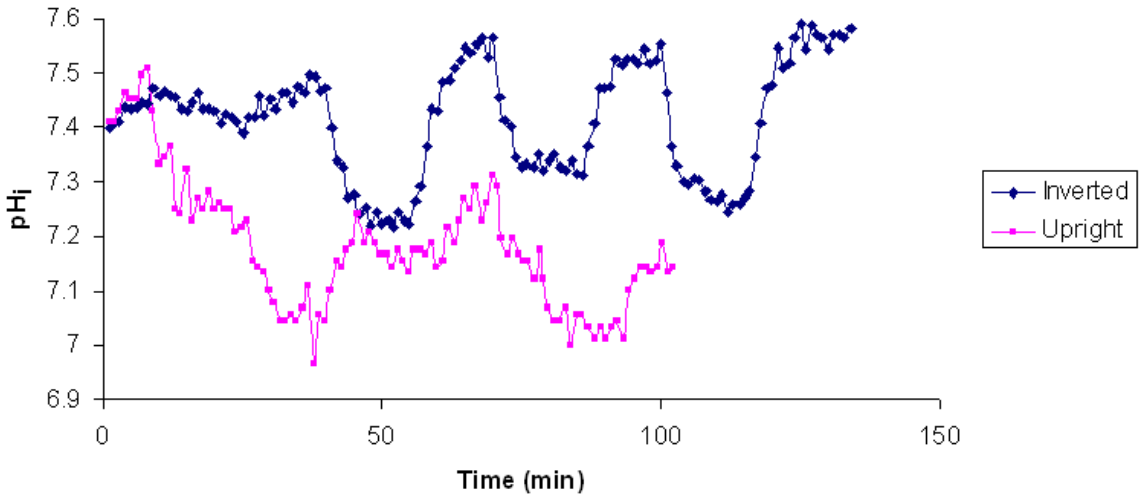
7.6
7.5
7.4
7.3
7.2
7.1
7
6.9
pHi
0
50
100
150
Time (min)
Inverted
Upright

CHAPTER VI

DISCUSSION

The overall goal of this project was to develop a technique that could hold intracellular pH constant in the face of an acid challenge (hypercapnic acidosis). The main conclusions of this study are that to minimize changes of pH_i:

A) Increasing the intracellular buffering power of individual neurons through the use of whole cell patching was fairly successful in NTS neurons.
B) Inducing a concurrent influx of weak base with hypercapnia through diffusion in whole slices was not successful in LC or NTS neurons.
C) Inducing a counter-balancing efflux of weak acid during hypercapnic exposure in whole slices was somewhat successful in LC and NTS neurons.
D) The ability to clamp pH_i is highly affected by diffusion of the weak acid both up to and into the cell. Success (better blunting) is improved with better superfusion (upright microscopes) and more permeable weak acids (caproic acid).

Buffering and the Whole Cell Technique

The most obvious way to hold pH_i relatively constant in a cell is to increase intracellular buffer. In this study, HEPES was used to increase the internal buffering power of neonatal NTS neurons. HEPES was loaded using an increased concentration of HEPES buffer (100mM) in the whole cell patch pipette into individual cells within brainstem slices. It has previously been reported that the use of HEPES-buffered internal solution (100, 70, and 40mM) was unsuccessful in fully clamping pH_i in LC neurons of neonatal rats, but the magnitude of the percent blunting was not investigated (Hartzler et al., 2008). In rat neonatal NTS neurons, the result is similar in that it did not fully prevent HA-induced intracellular acidification, but the reduction of the response was sizeable

nevertheless. There was reason to believe that internal buffering might work better in NTS than LC neurons because NTS cells are smaller and do not possess as many gap junctions, so there would not be as much buffer loss to other cells. The loading of HEPES would therefore require less time to diffuse throughout the soma to work. It was also speculated that the viscosity of HEPES buffer itself might play a role in its diffusion throughout the cytoplasm. The same investigators (Hartzler et al., 2008) additionally reported that replacing HEPES with another buffer, Trizma base (Tris[hydroxymethyl]amino-methane), similarly did not alter HA-induced acidification.

The biggest factor surrounding the use of intracellular buffering to blunt pH_i is getting the buffer into the cell at all. The approach used in this study was to employ the whole cell patch technique. Despite the advantages (see Literature Review), there are several disadvantages with the use of patching and the use of high levels of buffer as well: 1) To get sizeable pH_i blunting, the concentration of buffer must be very high and we cannot be sure whether this high concentration of buffer has other effects on the cell. 2) Buffering by its nature can blunt changes of pH but cannot regulate pH_i back to normal in response to an acid or base disturbance. Buffers thus will minimize the magnitude of an acid or alkaline challenge but otherwise cannot actively keep pH_i constant (Roos and Boron, 1981; Putnam and Roos, 1997). 3) In these experiments, whole cell patching loaded 10mM ("low HEPES") buffer into the cell. What effects this in itself has on true pH_i changes might introduce complications, so it is also better to use non-whole cell methods. For example, we see that in NTS neurons, the initial hypercapnia-induced pH_i change using HEPES buffer is about 0.12 pH unit using low HEPES (Fig. 12). Compare this with the other HA-induced pH_i changes of the other

experiments: 0.28 pH unit using inverted Na-ace (Fig. 15), 0.20 pH unit using TMA (Fig. 19), and 0.25 pH unit using Na-cap (Fig. 21). 4) Whole cell patching is an especially labor-intensive process which does not always work with every cell. There are potential obstacles such as "pipette drift" where the electrode tip may not stay attached to the cell, and impalement of the neuron can damage the cell and render it permanently unusable. 5) Whole cell patching only measures one cell at a time, making it an especially time-intensive process as each cell can require an hour or more to gather data. 6) In conjunction with point 5, chemosensitive neurons contained within chemosensitive brainstem areas only comprise a portion of each region, anywhere from 10 to 90%. In the LC, greater than 80% of its neurons are activated by hypercapnia but in the NTS only about 45% are activated by hypercapnia (Putnam 2001; Filosa et al., 2002; Conrad et al. 2009). This can make it difficult to achieve a patch of a chemosensitive neuron. Glial and other cells also exist within these regions, contributing to further heterogeneity and difficulty in determining which cells are chemosensitive. 7) As mentioned previously, the investigator also cannot reversibly alter the response of the neuron if loading buffer via the whole cell technique. Once a cell is patched, the cell is either blunted or not since the investigator cannot remove the pipette or change intracellular solution mid-patch. With these disadvantages, we thus endeavored to develop other techniques that did not involve whole cell patching and that would make pH_i clamping easier in a large population of cells at once.

Weak Base Loading

In exposing a cell to weak base simultaneously with exposure tohypercapnic acidosis, the cell experiences a simultaneous influx of acid (in this study as CO_2) and

base (in this study as TMA) that should theoretically result in no net change of pH_i. The advantages of this approach are that it is much easier and obviously less time, equipment, and labor-intensive. Further, it, in theory, will work on all the cells being exposed. The major disadvantage, however, is that it worked very poorly. Although it has been previously reported that a weak base diffusion technique worked well with both whole cell or perforated patch configurations in mice macrophages (Grinstein et al., 1994), direct diffusion of the weak base without patching seems to work much less successfully. We currently have no full explanation for this behavior but it may be that TMA is poorly permeable across the membrane of nerve cells, or that the slice limits diffusion of TMA up to the cell so substantially that the cells do not actually experience much weak-base loading.

Other disadvantages of weak base use for pH_i blunting include the tendency for weak bases to behave like potassium ions and thereby result in depolarization of the cell membrane potential (Hartzler et al., 2008). This is especially problematic when the membrane potential is a critical measure of the response of the cell, as with the studies of chemosensitive neurons. Thus, it is impractical to use weak bases for pH blunting in studies of the relationship of changes of pH_i with neuronal firing rate.

Weak Acid Loading

We have previously observed that chemosensitive neurons tolerate the loading of weak acids well and maintain normal firing rate responses to hypercapnia (Hartzler et al., 2008). Blunting due to weak acid loading is based on countering the acidification due to hypercapnia with a counterbalancing efflux of a weak acid. To explain again: by initially loading a neuron with a weak acid (HA_i), such as Na-ace or Na-cap used in this study,

simultaneous exposure to hypercapnia while lowering the concentration of HA on the outside (HA_o) to create an efflux of HA, will thus remove H^+ from the cell at the same time hypercapnia is inducing an increase in internal H^+. This will lead to a blunting of the pH_i change normally induced by hypercapnia. This technique also allows for the pH_i change induced by hypercapnia to either be blunted or to result in a fall of pH_i. By keeping the concentration of HA high outside of the cell, weak acid will not efflux and the unchallenged response of a fall of pH_i in response to hypercapnia can be recorded. Thus manipulation of the concentration of weak acid outside the cell enables the investigator to either clamp pH_i or not within the same cell. We were therefore able to both clamp and not clamp within an experimental run within the same cell, allowing a cell to serve as its own control.

This technique has proved useful in LC neurons, where the chemosensitive response was found to be maintained in the face of hypercapnic acidosis despite a clamped, and therefore unchanged, pH_i (Hartzler et al., 2008). These data resulted in the dramatic finding that while a decrease of pH_i was *sufficient* for chemosensitive signaling in LC neurons, it was not *necessary*, a finding in marked contrast to the original model of chemosensitive signaling as shown in Figure 3. This demonstrates how useful a pH_i clamping technique can be to studies of the role of changes of pH_i in cellular processes. Hartzler et al. (2008) loaded the weak acid, Na-acetate, directly with a whole cell patch pipette containing high concentrations of Na-acetate.

In the current study, we tried to adapt this technique to slices in an attempt to blunt several cells at once, but we encountered difficulties. Our initial attempts employed Na-acetate given its previous success, but we found minimal blunting with Na-acetate

even in LC neurons (Figures 14, 15 and 16). To explain this, we first hypothesized that not enough acid was getting into the cell to allow an adequate efflux to counter hypercapnic influx. Measuring how much acid was initially loaded could be determined by the magnitude of the initial acidification seen upon diffusive loading of the cell (e.g. Figure 14). A greater initial acidification, therefore, might mean more weak acid was loaded into the neuron. Plots expressing the relationship between blunting and initial pH_i change using an inverted microscope in both the NTS and LC are shown in Figures 18 and 23 for Na-acetate and Na-caproate, respectively. However, counter to our prediction, in all cases no strong relationship between initial acid loading and final % blunting is suggested via these graphs. With Na-ace, blunting and initial loading are inversely related, with blunting increasing with less acid loading exhibited by the negative slope. The case is similar in LC neurons using Na-cap, although the slope is slightly positive with Na-cap NTS cells. With both acids, however, there does not appear to be an correlation in either direction. This lack of strong correlation suggests that our initial hypothesis must be incorrect, that is, the initial rate of acidification must not correlate well with the degree of acid loading. One possible reason why this is the case may be that the acidification may be blunted by the presence of pH_i recovery in some cells (e.g. see Figure 14, lower trace) which would weaken any correlation between initial acidification and % blunting. In addition, the degree of initial acidification may be more a function of the initial buffering power of the cell than the degree of acid loading. Thus, any cell with a small degree of initial acidification may be well buffered and this buffering may contribute to an apparent slightly better blunting of hypercapnic acidosis.

FIGURE 28. Chemical structures of sodium acetate (Na-ace) and sodium caproate (Na-cap). Na-ace, on top, is a two carbon molecule. Na-cap, on bottom (also Na-hexanoate, caproic acid, or hexanoic acid), is a six carbon molecule related in structure to Na-ace. Longer carbon chains make molecules more lipophilic. Consequently, Na-cap should be better able to diffuse across the neuronal membrane and achieve better weak acid loading.

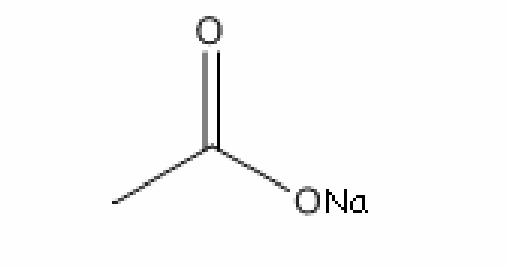

sodium acetate

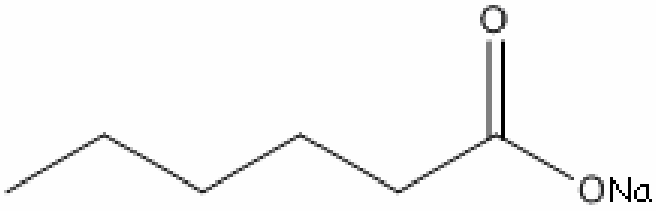

sodium caproate

Whatever the explanation, it appears that weak acid loading is insufficient to accomplish a high degree of blunting of hypercapnic acidosis.

We therefore considered that the low blunting results were due to loading difficulties across the neuronal membrane. One possible reason for poor loading is that acetic acid may not be highly permeable across the neuronal membrane. To test this, we identified a weak acid that should have a higher permeability to biological membranes, and thus selected a weak acid that should be considerably more hydrophobic than acetic acid. This was achieved by switching Na-ace for a similar molecule with a longer carbon chain (Figure 28). Na-caproate has four more carbons (with a total of six) compared to Na-ace, and was also chosen because it, although more expensive than acetate, was relatively cheaper than any of the other analogues and did not present us with any solubility issues. When the experiments were run again, Na-caproate approximately doubled the blunting percentage in both NTS and LC neurons. This suggests that the degree of pH_i blunting is probably limited by the ability of the weak acid to diffuse into the cell. Therefore, to achieve as high a blunting as possible, one should select a weak acid with as high a membrane permeability as possible that can still be dissolved in aCSF at a sufficiently high (tens of mM) concentration.

Despite the improved buffering with caproic acid, it still did not blunt pH_i more than 50%. We thus next considered the ability of the weak acid not only to diffuse into the cell, but up to the cell itself. Weak acid must also travel to the slice and through the brainstem tissue and anatomical meshwork that surrounds the neurons, including other neuronal cell bodies, neuronal processes, and glial cells. These diffusion barriers were addressed in part by switching the setup configuration from an inverted microscope to an

upright microscope (see Figure 24). Upright objectives view neurons that are more directly exposed to the flow of solution and are thus better superfused than the cells underneath viewed by inverted microscopes. In these studies, Na-acetate was again utilized to compare the blunting with the original weak-acid diffusion experiments using the inverted microscope. The results, like Na-caproate, doubled the blunting percentage, indicating strongly that diffusion limitations created by the set up can undoubtedly limit the ability of weak acid to load into the cell. Thus, the use of the upright microscope is clearly preferable to the use of an inverted microscope in studies to attempt pH_i clamping in the face of acid loads. These studies show that the ability to clamp pH_i is strongly dependent on both the ability of the weak acid to perfuse up to the cell as well as on its ability to diffuse into the neuron itself.

We note that neither the use of a highly permeable weak acid nor the use of the upright microscope alone resulted in greater than 50% blunting of hypercapnia-induced neuronal acidification. However, blunting pH_i under both conditions could theoretically yield even greater blunting percentages, and it would be of interest to try the two methods in concert. Preliminary data in both regions have shown that the blunting does improve when using caproic acid and the upright microscope, but not by very much. In NTS neurons ($n = 26$), percent blunting amounted to $54.8 \pm 2.9\%$, and in LC neurons ($n = 21$), percent blunting was $60.0 \pm 2.7\%$ (Rui Feng, personal communication). These data suggest that when used in concert, the effects of caproic acid and the upright microscope are not additive. Our data also show that neither of the two techniques eliminate diffusion limitations associated with the need for the weak acid to diffuse through the surrounding tissue. In this regard, it is interesting that one set of cells within one slice exhibited near

total pH_i clamping (Figure 17). It may be that in this slice, neurons very close to the surface survived slicing and were easily visualized, and that the limitations of diffusion through the surrounding tissue were minimal. If this is the case, given that this experiment was done with acetic acid loading and using the inverted microscope, it would suggest that diffusion through the surrounding tissue could represent a major limitation to the loading of weak acid into neurons and thus a major limitation in the attempts to clamp pH_i.

It should also be noted that in some of our experiments, the superfusate used contained high magnesium and low calcium in order to block chemical synaptic transmission (SNB). We do not believe that the use of SNB altered the effects of the blunting experiments in comparison with the use of aCSF. Preliminary data using aCSF suggest that this is true: in NTS neurons (n = 30), blunting percentage was 19.5 ± 2.6%, and in LC neurons (n = 19), blunting percentage was 27.3 ± 3.5% (Mehak Goel, personal communication). These values are comparable to the results of both regions from the inverted Na-acetate experiments done in the presence of SNB reported in this thesis.

In summary, we have explored various techniques to hold intracellular pH constant during hypercapnic acidosis in chemosensitive regions of the neonatal rat brainstem, both on the level of the individual neuron as well as in the entire slice. We conclude that intracellular buffering with HEPES through the use of whole cell patching blunts pH_i rather successfully in single cells but does not clamp it completely. We also conclude that simultaneous loading of neurons within a slice with concurrent acid and base does not work to blunt pH_i. In contrast, loading a neuron with weak acid to efflux against CO_2 influx can work to blunt pH_i considerably if the weak acid is relatively

permeable to the cellular membrane and the cell is well-superfused. It is probably also beneficial to image cells as close to the surface of the slice as possible. Thus, we believe that with the appropriate set of conditions it will be possible to nearly completely clamp pH_i in response to hypercapnic acidosis in numerous cells within a slice.

CHAPTER VII

FUTURE DIRECTIONS

The results of this thesis suggest numerous future studies that would contribute to the development of refined techniques for successful intracellular pH clamping. With the success of these techniques, a wide scope of further work would benefit from the ability to blunt $pH_{i,}$ not only in chemosensitive neurons in the brainstem, but also a broad range of cell models in which pH_i may play an important signaling role. Because intracellular pH is such a fundamental component of almost all living cells, these methods would be of great use to address current research, examples of which are elaborated upon in this section.

We have shown that both superfusion and diffusion limitations play large roles in the ability to fully blunt acid changes in slices. The most obvious start for future work would be to improve each of these criterion to develop a technique for complete clamping of intracellular pH in the whole slice without whole cell patching. For example, Na-caproate could be substituted by another weak acid with an even longer carbon chain to increase the permeability of the weak acid across the neuronal membrane. However, the weak acid would have to be carefully selected to prevent solubility difficulties; molecules with more carbons might be too lipophilic to adequately dissolve at high concentrations in aCSF. In regards to superfusion, a two-sided superfusion technique could be utilized such that *both* sides of the brainstem slice would be directly exposed to the solution. In two-sided superfusion, the slice is not held to the bottom of the Plexiglas stage as previously described (see Materials and Methods), but immobilized by a nylon mesh and/or grid on both surfaces (D'Agostino et al., 2007). This method allows for direct contact with superfusate for neurons imaged either from the top or bottom of the experimental chamber. However, some visualization problems may occur because the

slice is thus raised above the stage to permit solution flow underneath. When utilized with an inverted scope to study superoxide production in hippocampal neurons, it was found that the change in working distance limited the use of certain objectives, so only lower magnifications could be used to see individual cells (D'Agostino et al., 2007). One could also use even thinner slices than the 300μm thickness used in this thesis to allow for better superfusion. Other possibilities include lowering the concentration of extracellular weak acid even more, below 16.16mM, to produce a greater efflux of weak acid, or use 10% CO_2 instead of a 15% acid challenge to improve blunting. An even better method that would potentially eliminate perfusion restrictions altogether would be to not use slices at all, but cultured or freshly dissociated cells. This would be the most direct way of all, since superfusate would not have to diffuse through the tissue to reach the neurons.

Should easier, successful pH_i clamping methods in whole slices manifest, much work in the respiratory field alone would benefit from such a technique. As described in the Literature Review, questions remain as to what precise role pH_i plays in the central chemosensitive response. One future area of research would be to investigate this role by clamping pH_i and measuring its effect on the firing rate response to hypercapnia as done with LC neurons by Hartzler et al. (2008), but repeated in nerons from the NTS, RTN, the medullary raphé, and/or any other potentially chemosensitive region. This would be significant not only to clarify the function of pH_i in neurons from each region but to establish whether or not chemosensitive signaling mechanisms differ between neurons from different regions. Another area of work would be to blunt pH_i and test those effects on the chemosensitive response in adult rats. The chemosensitive response appears

unchanged throughout the development of NTS neurons as neonatal rats mature (Conrad et al., 2009), but it would be interesting to assess whether these results are due to a lack of change in cellular signaling during the aging process. The investigator would compare how pH_i functions between adults and neonates with the rest of the respiratory network uniquely developed at those stages.

It would also be likely for such pH_i blunting methods to be useful in other non-respiratory related cell models where intracellular pH plays a significant role. For example, one such future direction would be to examine pH_i's relationship with bicarbonate and CO_2 in bicarbonate reabsorption in the proximal tubule. In a study by Zhao et al. (2003), bicarbonate reabsorption was investigated by manipulating basolateral $[CO_2]$ and $[HCO_3^-]$ in several bath solutions and the resultant reabsorption of bicarbonate studied. However, these measurements yielded consequent changes in pH_i as well. When the bath solution contained minimal CO_2, HCO_3^- reabsorption decreased but pH_i increased; when the bath solution contained minimal HCO_3^-, HCO_3^- reabsorption increased but pH_i decreased. Thus, one hypothesis that explains why this occurs suggests that the isolated removal of basolateral $HCO3^-/CO_2$ causes a pH_i increase that in turn lowers HCO_3^- reabsorption. If pH_i could be clamped in renal proximal tubule cells to see the effect on bicarbonate reabsorption, this hypothesis could be tested.

Another area of research where pH_i clamping might be useful is in the study of intracellular pH and free fatty acid (FFA) diffusion in adipocytes. Adipocytes function to store energy in the form of triglycerides through FFAs that move into and out of the cell. The mechanism that drives FFA diffusion is yet undetermined, though a proportional correlation between a drop in intracellular pH and diffused FFAs has been reported

(Civelek et al., 1996). In this study, it was suggested that this resultant intracellular acidification may play a role in the signaling mechanism for nutrient energy storage, a hypothesis that could be clarified by pH_i clamping experiments. For example, an investigator could ask how a constant intracellular pH affects FFA diffusion in the adipocyte environment, as pH_i has been measured as a function of intracellular levels of FFA, and how that same clamped pH_i affects the overall storage of triglycerides. It would be of use, therefore, to determine how the acidic environment necessarily affects adipocyte function. A hypothesis suggesting that intracellular acidosis plays a necessary part in energy storage could thus be examined.

A third area where these techniques would be useful is in acid detection in taste receptor cells. One of the mechanisms suggested by which acids activate taste receptors is through stimulus-invoked changes of pH_i. According to data in DeSimone et al. (2001), pH_i recovery of mammalian taste receptors occurs when extracellular pH is held constant, but pH_i recovery does not occur when pH_i changes are induced by decreasing extracellular pH. These are characteristics of a pH-sensing cell and contribute to the hypothesis that a decrease in taste receptor cell pH_i may be an essential step in sour taste transduction. If pH_i could be clamped in these cells, this theory could be tested, thereby observing how the subsequent steps in the process leading to neurotransmitter release and ultimately the sensation of sour taste are affected by pH_i change.

Yet a fourth area of future research that could benefit from pH_i clamping would be to investigate the dynamics of intracellular and extracellular pH and their differential characteristics within cancer cells. Interestingly, cancer cells are proposed to have a homeostatic acid-base disturbance that is completely different from acid-base balances

observed in regular tissue. Cancer cells have a reversal of the pH gradient typically seen in normal cells that results in intracellular alkalosis, a characteristic increasingly considered to be a hallmark of malignant cells (Harguindey et al., 2005; 2009). Recent research has suggested that several proton export transporters drive the initiation and progression of this pH reversal and that the inhibition of these mechanisms may be promising for the development of specific inhibitors as anti-cancer therapeutics. Adapting the weak-acid diffusion technique to modify pH_i in malignant cells over a longer time frame in cultured cancer cells might help to further clarify the potential role of intracellular pH changes in the control of growth of malignant cells *in vitro.*

In this thesis, we have blunted intracellular pH in two chemosensitive regions of the brainstem during hypercapnic acidosis, and have developed preliminary means of fully clamping pH_i in central chemosensitive cells in brainstem slices. Blunting pH_i in slices would be valuable in studying the involvement of pH_i in chemosensitive signaling. However, as suggested, the ability to clamp pH_i would be advantageous for other cellular systems where changes of pH_i are important as well. In almost any situation where pH_i is suggested as a signal in cellular function, the broad applicability of these techniques will be apparent.

CHAPTER VIII

BIBLIOGRAPHY

Alheid, GF., Milsom, WK., McCrimmon, DR., 2004. Pontine influences on breathing: an overview. 143(2-3):105-14.

Ballantyne, D., Andrzejewski, M., Mückenhoff, K., Scheid, P., 2004. Rhythms, synchrony and electrical coupling in the Locus coeruleus. 143(2-3):199-214.

Ballanyi, K., Mückenhoff, K., Bellingham, MC., Okada, Y., Scheid, P., Richter, DW., 1994. Activity-related pH changes in respiratory neurones and glial cells of cats. Neuroreport. 6(1):33-6.

Baxter, KA., Church, J., 1996. Characterization of acid extrusion mechanisms in cultured fetal rat hippocampal neurones. J Physiol. 493 (Pt 2):457-70.

Bayliss, DA., Talley, EM., Sirois, JE., Lei, Q., 2001. TASK-1 is a highly modulated pH-sensitive "leak" K(+) channel expressed in brainstem respiratory neurons. Respir Physiol. 129(1-2):159-74.

Berger, MG., Vandier, C., Bonnett, P., Jackson, WF., and Rusch, N., 1998. Intracellular acidosis differentially regulates Kv channels in coronary and pulmonary vascular muscle. Am J Physiol. 275 (4 Pt 2):H1351-9.

Bevensee, MO**.,** Schwiening, CJ**.,** Boron, WF., 1995. Use of BCECF and propidium iodide to assess membrane integrity of acutely isolated CA1 neurons from rat hippocampus. J Neurosci Methods. 58(1-2):61-75.

Bevensee, MO., Cummins, TR., Haddad, GG., Boron, WF., Boyarsky, G., 1996. pH regulation in single CA1 neurons acutely isolated from the hippocampi of immature and mature rats. J Physiol. 494 (Pt 2):315-28.

Biancardi, V., Bícego, KC., Almeida, MC., Gargaglioni, LH., 2008. Locus coeruleus noradrenergic neurons and CO2 drive to breathing. 455(6):1119-28.

Boron, WF., De Weer, P., 1976. Intracellular pH transients in squid giant axons caused by CO2, NH3, and metabolic inhibitors. J Gen Physiol. 67(1):91-112.

Boron, WF., Boyarsky, G., Ganz, M., 1989. Regulation of intracellular pH in renal mesangial cells. Ann N Y Acad Sci. 574:321-32.

Bouyer, P., Bradley, SR., Zhao, J., Wang, W., Richerson, GB., Boron, WF., 2004. Effect of extracellular acid-base disturbances on the intracellular pH of neurones cultured from rat medullary raphe or hippocampus. J Physiol. 559 (Pt 1):85-101.

Buckler, KJ., Vaughan-Jones, RD., Peers, C., Lagadic-Gossmann, D., Nye, PC., 1991a. Effects of extracellular pH, PCO2 and HCO3- on intracellular pH in isolated type-I cells of the neonatal rat carotid body. J Physiol. 444:703-21.

Buckler, KJ., Vaughan-Jones, RD., Peers, C., Nye, PC., 1991b. Intracellular pH and its regulation in isolated type I carotid body cells of the neonatal rat. J Physiol. 436:107-29.

Chambers-Kersh L, Ritucci NA, Dean JB, Putnam RW., 2000. Response of intracellular pH to acute anoxia in individual neurons from chemosensitive and nonchemosensitive regions of the medulla. Adv Exp Med Biol. 475:453-64.

Chelser, M., 2003. Regulation and modulation of pH in the brain. Physiol Rev. 83(4):1183-221.

Church, J., Baxter, KA., McLarnon, JG., 1998. pH modulation of Ca2+ responses and a Ca2+-dependent K+ channel in cultured rat hippocampal neurones. J Physiol. 511 (Pt 1):119-32.

Coates, EL., Li, A., Nattie, E., 1993. Widespread sites of brain stem ventilatory chemoreceptors. J Appl Physiol. 75(1):5-14.

Conrad, SC., Nichols, NL., Ritucci, NA., Dean, JB., Putnam RW., 2009. Development of chemosensitivity in neurons from the nucleus tractus solitarii (NTS) of neonatal rats. Respir Physiol Neurobiol.166(1):4-12.

Counillon, L., Pouysségur, J., 2000. The expanding family of eucaryotic Na(+)/H(+) exchangers. J Biol Chem. 275(1):1-4.

Cowan, AI., Martin, RL., 1995. Simultaneous measurement of pH and membrane potential in rat dorsal vagal motoneurons during normoxia and hypoxia: a comparison in bicarbonate and HEPES buffers. J Neurophysiol. 74(6):2713-21.

Civelek, VN., Hamilton, JA., Tornheim, K., Kelly, KL., Corkey, BE., 1996. Intracellular pH in adipocytes: effects of free fatty acid diffusion across the plasma membrane, lipolytic agonists, and insulin. Proc Natl Acad Sci U S A. 93(19):10139-44.

D'Agostino, DP., Putnam, RW., Dean, JB., 2007. Superoxide (*O2-) production in CA1 neurons of rat hippocampal slices exposed to graded levels of oxygen. J Neurophysiol. 98(2):1030-41.

Dean, JB., Lawing, WL., Millhorn, DE., 1989. CO2 decreases membrane conductance and depolarizes neurons in the nucleus tractus solitarii. Exp Brain Res.76(3):656-61.

Dean, JB., Bayliss, DA., Erickson, JT., Lawing, WL., Millhorn, DE., 1990. Depolarization and stimulation of neurons in nucleus tractus solitarii by carbon dioxide does not require chemical synaptic input. Neuroscience. 36(1):207-16.

DeSimone, JA., Lyall, V., Heck, GL., Feldman, GM., 2001. Acid detection by taste receptor cells. Respir Physiol. 129(1-2):231-45.

Diarra, A., Sheldon, C., Brett, CL., Baimbridge, KG., Church, J., 1999. Anoxia-evoked intracellular pH and Ca2+ concentration changes in cultured postnatal rat hippocampal neurons. Neuroscience. 93(3):1003-16.

Doi, T. Fakler, B., Schultz, JH., Schulte, U., Brändle, U., Weidmann, S., Zenner, HP., Lang, F., Ruppersberg, JP., 1996. Extracellular K+ and intracellular pH allosterically regulate renal Kir1.1 channels. J Biol Chem. 271(29):17261-6.

Filosa, JA., Dean, JB., Putnam, RW., 2002. Role of intracellular and extracellular pH in the chemosensitive response of rat locus coeruleus neurones. J Physiol. 541 (Pt 2):493-509.

Filosa, JA., Putnam, RW., 2003. Multiple targets of chemosensitive signaling in locus coeruleus neurons: role of K+ and Ca2+ channels. Am J Physiol Cell Physiol. 284(1):C145-55.

Fung, ML., St John, WM., 1994. Neuronal activities underlying inspiratory termination by pneumotaxic mechanisms. Respir Physiol. 98(3):267-81.

Gan, BS., Krump, E., Shrode, LD., Grinstein, S., 1998. Loading pyranine via purinergic receptors or hypotonic stress for measurement of cytosolic pH by imaging. Am J Physiol. 275 (4 Pt 1):C1158-66.

Goldstein, JI., Mok, JM., Simon, CM., Leiter, JC., 2000. Intracellular pH regulation in neurons from chemosensitive and nonchemosensitive regions of Helix aspersa. Am J Physiol Regul Integr Comp Physiol. 279(2):R414-23.

Grinstein, S., Putnam, RW., 1994. Measurement of intracellular pH. In: Schafer, JA., Giebisch, G., Kristensen, P., Ussing, HH., (Eds.), Methods in Membrane and Transporter Research. R.G. Landes Company, Austin, Texas, pp.113–141.

Grinstein, S., Romaneck, R., Rostein, OD., 1994. Method for manipulation of cytosolic pH in cells clamped in the whole cell or perforated-patch configurations. Am J Physiol Cell Physiol. 267, C1152-C1159.

Harguindey, S., Orive, G., Luis Pedraz, J., Paradiso, A., Reshkin, SJ., 2005. The role of pH dynamics and the Na+/H+ antiporter in the etiopathogenesis and treatment of cancer. Two faces of the same coin--one single nature. Biochim Biophys Acta.1756(1):1-24.

Harguindey, S., Arranz, JL., Wahl, ML., Orive, G., Reshkin, SJ., 2009. Proton transport inhibitors as potentially selective anticancer drugs. Anticancer Res. 29(6):2127-36.

Hartzler, LK., Dean JB., Putnam, RW., 2008. The Chemosensitive Response of Neurons from the Locus Coeruleus (LC) to Hypercapnic Acidosis with Clamped Intracellular pH. In: Poulin, M., Wilson, RJA., (Eds.), Integration in respiratory control: from genes to systems. Springer, New York. Vol. 605. pp. 333-337.

Huang, RQ., Erlichman, JS., Dean, JB., 1997. Cell-cell coupling between CO2-excited neurons in the dorsal medulla oblongata. Neuroscience. 80(1):41-57.

Kersh, AE., Hartzler, LK., Havlin, K., Belcastro, B., Nanagas, VC., Kalra, A., Chua, J., Whitesell, R., Ritucci, NA., Dean, JB., Robert W. Putnam, RW., 2009. pH regulating transporters in rat brainstem neurons. Am J Physiol. In revision.

Khuri RN, Agulian SK, Abdulnour-Nakhoul S, Nakhoul NL., 1992. Electrochemical potentials of potassium in skeletal muscle under different metabolic states. J Cell Physiol. 153(3):534-8.

Kiwull-Schöne, H., Wiemann, M., Frede, S., Bingmann, D., Wirth, KJ., Heinelt, U., Lang, HJ., Kiwull, P., 2001. A novel inhibitor of the Na+/H+ exchanger type 3 activates the central respiratory CO2 response and lowers the apneic threshold. Am J Respir Crit Care Med. 164(7):1303-11.

Klöckner, U., Isenberg, G., 1994. Intracellular pH modulates the availability of vascular L-type Ca2+ channels. J Gen Physiol. 103(4):647-63.

Krause, KL., Forster, HV., Kiner, T., Davis, SE., Bonis, JM., Qian, B., Pan, LG., 2009. Normal breathing pattern and arterial blood gases in awake and sleeping goats after near total destruction of the presumed pre-Botzinger complex and the surrounding region. J Appl Physiol. 106(2):605-19.

Lassen, NA., 1990. Is central chemoreceptor sensitive to intracellular rather than extracellular pH? Clin Physiol. 10(4):311-9.

Leiter, LC., 2009. Intrinsic chemosensitivity: How is it measured; what does it mean; and how does it help us understand the ventilatory response to CO_2? Respir Physiol Neurobiol. 166(1):13-15.

Li, ZY., Xia, BL., Huang, CJ., 1992. Effects of microinjection of L-glutamate into locus coeruleus complex area on respiration. 12(4):205-8.

Martino, PF., Putnam, RW., 2007. The effect of 4-aminopyradine (4AP) on the hypercapnic response of locus coeruleus (LC) neurons. Soc Neurosci. Abstrs.

Miller, P., Peers, C., Kemp, PJ, 2004. Polymodal regulation of hTREK1 by pH, arachidonic acid, and hypoxia: physiological impact in acidosis and alkalosis. Am J Physiol Cell Physiol. 286(2):C272-82.

Mizusawa, A., Ogawa, H., Kikuchi, Y., Hida, W., Shirato, K., 1995. Role of the parabrachial nucleus in ventilatory responses of awake rats. J Physiol. 489 (Pt 3):877-84.

Muñoz-Cabello, AM., Toledo-Aral, JJ., López-Barneo, J., Echevarría, M., 2005. Rat adrenal chromaffin cells are neonatal CO2 sensors. J Neurosci. 25(28):6631-40.

Nattie, E., 1999. CO2, Brainstem chemoreceptors and breathing. Prog Neurobiol. 59(4):299-331.

Nattie, E., 2000. Multiple sites for central chemoreception: their roles in response sensitivity and in sleep and wakefulness. Respir Physiol. 122(2-3):223-35.

Nichols, NL., Hartzler, LK., Conrad, SC., Dean, JB., Putnam, RW., 2008. Intrinsic chemosensitivity of individual nucleus tractus solitarius (NTS) and locus coeruleus (LC) neurons from neonatal rats. Adv Exp Med Biol. 605:348-52.

Nicola, PA., Taylor, CJ., Wang, S., Barrand, MA., Hladky, SB., 2008. Transport activities involved in intracellular pH recovery following acid and alkali challenges in rat brain microvascular endothelial cells. Pflugers Arch. 456(5):801-12.

Nottingham, S., Leiter, JC., Wages, P., Buhay, S., Erlichman, JS., 2001. Developmental changes in intracellular pH regulation in medullary neurons of the rat. Am J Physiol Regul Integr Comp Physiol. 281(6):R1940-51.

Orlowski, J., Grinstein, S., 2004. Diversity of the mammalian sodium/proton exchanger SLC9 gene family. Pflugers Arch. 447(5):549-65.

Oyamada, Y., Ballantyne, D., Mückenhoff, K., Scheid, P., 1998. Respiration-modulated membrane potential and chemosensitivity of locus coeruleus neurones in the in vitro brainstem-spinal cord of the neonatal rat. J Physiol. 513 (Pt 2):381-98.

Pocock, G., Richards, CD., 1992. Hydrogen ion regulation in rat cerebellar granule cells studied by single-cell fluorescence microscopy. Eur J Neurosci. 4(2):136-143.

Putnam, RW., Roos A, 1997. Intracellular pH. In: Hoffman, JF., Jamieson, JD., (Eds.), Handbook of Physiology: Cell Physiology. Oxford Univer. Press, New York, pp. 389–440.

Putnam, RW., 2001. Intracellular pH regulation of neurons in chemosensitive and nonchemosensitive areas of brain slices. Respir Physiol. 129(1-2):37-56.

Putnam, RW., Filosa, JA., Ritucci, NA., 2004. Cellular mechanisms involved in CO(2) and acid signaling in chemosensitive neurons. Am J Physiol Cell Physiol. 287(6):C1493-526.

Raley-Susman, KM., Sapolsky, RM., Kopito, RR., 1993. Cl-/HCO3- exchange function differs in adult and fetal rat hippocampal neurons. Brain Res. 614(1-2):308-14.

Ritucci, NA., Erlichman, JS., Dean, JB., Putnam, RW., 1996. A fluorescence technique to measure intracellular pH of single neurons in brainstem slices. J Neurosci Methods. 68(2):149-63.

Ritucci, NA., Dean, JB., Putnam, RW., 1997. Intracellular pH response to hypercapnia in neurons from chemosensitive areas of the medulla. Am J Physiol. 273 (1 Pt 2):R433-41.

Ritucci, NA., Chambers-Kersh, L., Dean, JB., Putnam, RW., 1998. Intracellular pH regulation in neurons from chemosensitive and nonchemosensitive areas of the medulla. Am J Physiol. 275 (4 Pt 2):R1152-63.

Ritucci, NA., Erlichman, JS., Leiter, JC., Putnam, RW., 2005. Response of membrane potential and intracellular pH to hypercapnia in neurons and astrocytes from rat retrotrapezoid nucleus. Am J Physiol Regul Integr Comp Physiol. 289(3):R851-61.

Romero, MF., Fulton, CM., Boron, WF., 2004. The SLC4 family of HCO 3 - transporters. Pflugers Arch. 447(5):495-509.

Roos, A., Boron, WF., 1981. Intracellular pH. Physiol Rev. 61(2):296-434.

Schewe, B., Schmälzlin, E., Walz, B., 2008. Intracellular pH homeostasis and serotonin-induced pH changes in Calliphora salivary glands: the contribution of V-ATPase and carbonic anhydrase. J Exp Biol. 211 (Pt 5):805-15.

Schwiening, CJ., Boron, WF., 1994. Regulation of intracellular pH in pyramidal neurones from the rat hippocampus by Na(+)-dependent Cl(-)-HCO3- exchange. J Physiol. 475(1):59-67.

Smith, GA., Brett, CL., Church, J., 1998. Effects of noradrenaline on intracellular pH in acutely dissociated adult rat hippocampal CA1 neurones. J Physiol. 512 (Pt 2):487-505.

Spyer, MK., 2009. To breathe or not to breathe? That is the question. Exp Physiol. 94(1):1-10.

Song, G., Poon, CS., 2009. Lateral parabrachial nucleus mediates shortening of expiration and increase of inspiratory drive during hypercapnia. Respir Physiol Neurobiol. 165(1):9-12.

Summers, BA., Overholt, JL., Prabhakar, NR., 2002. CO(2) and pH independently modulate L-type Ca(2+) current in rabbit carotid body glomus cells. J Neurophysiol. 88(2):604-12.

Stewart, RE., Lyall, V., Feldman, GM., Heck, GL., DeSimone, JA., 1998. Acid-induced responses in hamster chorda tympani and intracellular pH tracking by taste receptor cells. Am J Physiol. 275 (1 Pt 1):C227-38.

Takahashi, KI., Copenhagen, DR., 1996. Modulation of neuronal function by intracellular pH. Neurosci Res. 24:109-116.

Taylor, CJ., Nicola, PA., Wang, S., Barrand, MA., Hladky, SB., 2006. Transporters involved in regulation of intracellular pH in primary cultured rat brain endothelial cells. J. Physiol. 576(Pt 3):769-85.

Thomas, RC., 1974. Intracellular pH of snail neurons measured with a new pH-sensitive glass micro-electrode. J Physiol. 238:159-180.

Tombaugh, GC., 1998. Intracellular pH buffering shapes activity-dependent Ca2+ dynamics in dendrites of CA1 interneurons. J Neurophysiol. 80:1702-1712.

Trapp, S., Lückermann M, Brooks PA, Ballanyi K., 1996. Acidosis of rat dorsal vagal neurons in situ during spontaneous and evoked activity. J Physiol. 496 (Pt 3):695-710.

Wang, W**.,** Richerson, GB**.,** 2000. Chemosensitivity of non-respiratory rat CNS neurons in tissue culture. Brain Res. 860(1-2):119-29.

Wegner, H., Reeh, PW., Brehm, S., Kreysel, HW., Steen, KH., 1996. Diltiazem blocks the pH-induced excitation of rat nociceptors together with their mechanical and electrical excitability in vitro. J Neurophysiol. 75: 1-10.

Wellner-Kienitz, MC., Shams, H., Scheid, P., 1998. Contribution of Ca2+-activated K+ channels to central chemosensitivity in cultivated neurons of fetal rat medulla. J Neurophysiol. 79(6):2885-94.

Wiemann, M., Baker, RE., Bonnet, U., Bingmann, D., 1998. CO2-sensitive medullary neurons: activation by intracellular acidification. Neuroreport. 9(1):167-70.

Wiemann, M., Bingmann, D., 2001. Ventrolateral neurons of medullary organotypic cultures: intracellular pH regulation and bioelectric activity. Respir Physiol. 129(1-2):57-70.

Yang, Z., Jiang, C., 1999. Opposite effects of pH on open-state probability and single channel conductance of kir4.1 channels. J Physiol. 520 (Pt 3):921-7.

Zhao, J., Zhou, Y., Boron, WF., 2003. Effect of isolated removal of either basolateral HCO-3 or basolateral CO2 on HCO-3 reabsorption by rabbit S2 proximal tubule. Am J Physiol Renal Physiol. 285(2):F359-69.